Optimization of Head and Duct Design for a Warehouse Vacuum Robot Using Computational Fluid Dynamics

by

Barbara Maia Araujo Lima

B.Sc., Chemical Engineering, Massachusetts Institute of Technology, 2016

Submitted to the Department of Mechanical Engineering in partial fulfillment of the requirements for the degree of

MASTER OF ENGINEERING IN ADVANCED MANUFACTURING AND DESIGN

at the

MASSACHUSETTS INSTITUTE OF TECHNOLOGY

September 2017

Signature of Author_____

Department of Mechanical Engineering
August 10, 2017

Certified by_____

Maria Yang
Associate Professor of Mechanical Engineering
Thesis Supervisor

Accepted by_____

Rohan Abeyaratne
Quentin Berg Professor of Mechanics
Chairman, Committee on Graduate Students

This page intentionally left blank

Optimization of Head and Duct Design for a Warehouse Vacuum Robot Using Computational Fluid Dynamics

by

Barbara Maia Araujo Lima

Submitted to the Department of Mechanical Engineering on August 11, 2017 in partial fulfillment of the requirements for the degree of Master of Engineering in Advanced Manufacturing and Design

ABSTRACT

This project focused on the development of a vacuum head and duct for integration into an automated robotic vacuum cleaning unit for warehouse and industrial applications. Although many autonomous cleaning robots are available on the market, very few are appropriate for industrial applications and those that are often have slow cleaning rates and bulky, impractical sizes. By computational fluid dynamics (CFD) simulations, prototyping, and testing, an improved option for such a robot was created with the capability of competing with current vacuums, a significantly smaller volume, and the ability to clean while moving at much faster speeds. The CFD was crucial in speeding up the iterative design process for the vacuum head as it eliminated the need for many physical iterations. Ultimately a second design is suggested but was not tested. Further recommendations are made as to what areas of improvement could be developed in the future.

Thesis Supervisor: Maria Yang
Title: Associate Professor of Mechanical Engineering

This page intentionally left blank

ACKNOWLEDGEMENTS

I would like to thank my family for supporting me and helping me get to where I stand today. In addition to that, I would also like to thank my teammates Benjamin Schilling, Jody Fu, and Youngjun Joh for putting in all the hard work and hours to complete our project. Prof. Maria Yang's guidance was vital to the success of this project. Jose Pacheco and Prof. David Hardt vision for this program and the projects this year inspired me to work hard in achieving my goals and making that vision a reality. I would like to thank all three of them for the support they have provided me throughout my pursuit of this degree and the completion of the project.

Lastly, I would like to thank all the industry experts for their support and belief in this project. The project could not have happened without Parris and Peter who sponsored the MEng program and partnered with MIT for this project. Jennifer and Jude provided great day-to-day guidance and expert insights that helped us overcome major obstacles along the way. Craig and the software team helped us pull the project together by providing expertise in areas where the MIT team had little to no prior experience. Dragan, Gabriel, and Allan passed on some useful knowledge from their prior experience and their constructive criticism and recommendations often pointed out important areas for improvement. Earl provided us with space to carry out the project to its full potential. Ron and Mark were of immense help in making our plans and ideas come to life.

This page intentionally left blank

TABLE OF CONTENTS

LIST OF FIGURES

LIST OF TABLES

This page intentionally left blank

CHAPTER 1: INTRODUCTION

Background

The purpose of this thesis project is to propose a design for the head and duct of an automatic cleaning robot that can be used in existing warehouses and fulfillment centers.

As automation expands into many areas of industry, there are now several providers of robots for transporting products within warehouses. These robots usually have the capability of picking up one or several products and transporting them within an allocated warehouse floor. The product is often placed in a specialized container to facilitate the robot's interaction with it. Depending on how the specific warehouse operates, product can also be grouped in these containers so that multiple products are transported in a single container. These robots will be referred to as carrier robots and usually have an allocated area within the warehouse in which they can operate – this will be called the robot-operated area. The carrier robots carry out tasks like bringing the containers from the warehouse floor to an area where desired products can be packaged and sent out and also taking incoming items to the appropriate storage location within the warehouse. Usually a human interacts with the carrier robot to either pick up an item from it for shipping preparation or to give it an item after it is ready for storage, but this is done only in designated areas where the interaction is well controlled and restricted so as to prevent harm to the robot or human. Humans are therefore generally not allowed to operate side-by-side with the robots in the robot-operated area. The carrier robots often move and can find and place items in the correct locations faster than human employees would so they can save time in the sorting operations of the warehouse. By using the carrier robots many warehouses are also able to save space and therefore money by grouping items more closely together than can be done with a human-operated warehouse. This is because the carrier robots can be used to quickly move items so as to move open space to where it is needed. For example, instead of having aisles that allow access to every item, the number of aisles in the warehouse could be halved and if something that is not accessible is needed, the carrier robots can move items so as to close an existing aisle and create another where

it is needed, therefore effectively moving the aisle by moving the other items in the warehouse.

Cleanliness of these robot-operated warehouses and areas is important in order to guarantee accurate navigation of the automated robots, especially if they rely on dead reckoning or on a navigation system that is set down on the warehouse floors and could deteriorate if covered by dirt. Cleaning of the robot-operated areas, however, is mostly done by human-operated machinery and since most existing robots are not safe for operation in the same space as human operators without strict control and safety mechanisms, cleaning often entails shutting down sections of the robot-operated areas until cleaning operations are completed. One possible solution to this loss of efficiency is to develop a second type of robot – a robot that continuously cleans the robot-operated area and can safely navigate the area along with the other carrier robots. This second type of robot will be referred to as a cleaning robot and was the focus of this project. Ideally the cleaning robot would not change the dynamics of the interactions or the area by its presence and would be able to navigate to all areas that the carrier robots can also access. It is crucial that the automated cleaning robot (or a team of them) be able to clean the entire robot-operated area well enough such that the level of human interaction and therefore carrier robot downtime decreases sufficiently to justify the cost of the cleaning robots.

Existing Products

There are many automated cleaning robots on the market, but only a small subset of them would be appropriate for use in a warehouse environment. Some of the specifications for commercially available automated cleaners for warehouse and/or industrial environments are shown below but most do not meet the functional requirements for operation in many warehouses due to their size. Many of these cleaners also currently operate on a randomized path methodology and it would take significant retrofitting of software to incorporate such a cleaning robot into a warehouse that already uses carrier robots. This is because the necessary precautions would have to be taken to prevent other robots from bumping into the cleaning robot either by knowing its position or by implementing sensor

technology. Additionally, the randomized path of the cleaner could also decrease its efficiency and change the carrier robot traffic and dynamics within the warehouse. The software implementation issue will likely be a problem even with the product developed in this project but the difference is that with a smaller cleaning robot more navigational flexibility can be achieved to adapt to the existing warehouse environment.

Table 1: Summary of existing robotic autonomous cleaners and their capabilities. Solution based technologies are those that use water, surfactants, or some type of liquid to clean.

Cleaner	DuoBot 1850[1]	SwingBoth 1650[2]	AeroBot 1850[3]	Makita RC200DZ[4,5,6,7]
Cleaning Technology	Solution and Vacuum	Solution	Vacuum	Vacuum
Brush Rotation Speed (RPM)	800	200	1390	Unknown
Waste Storage Capacity (gal)	14 + 1.15	14	10	0.66
Dimensions (height x width x length in in.)	43 x 32 x 48	43 x 32 x 48	43 x 34.5 x 50	34.6 x 26 x 33.5
Run Time (h)	4	4	4	3.33
Cleaning Pressure (lb.)	50	100	-	-
Cleaning Rate (sq. ft./h)	10,000	10,000	10,000	1615
Cleaning Width (in)	33.375	32	32	18.167
Noise (dBA)	65	65	65	64

Project Goals

Given the incompatibility of the commercially available automated cleaning robots with automated warehouse operations, the broad goal of the project carried out for this thesis work is to develop a functioning prototype of a more appropriate cleaning robot that could be incorporated into existing automated warehouses. To carry this out, an existing carrier robot was retrofitted to accommodate the necessary cleaning mechanisms.

Early in the project a choice was made to pursue vacuuming as the main mode of cleaning for the cleaning robot since most of the debris found in warehouses consists of regular dust

and cement dust. Surfactants that may have been used for washing the floors were ruled out as a main solution since these often leave thin films of water and/or remaining surfactant that could further deteriorate the navigation with dead reckoning. For special circumstances of product spill, surfactant-based solutions could be reconsidered in further studies but are likely not the best option for general cleaning. Such a study is amongst the recommended areas for further work at the end of this thesis.

Vacuums generally contain 6 main components: brush, head, duct, debris storage bin, filters, and blowers/fans. A roller brush sits in the head and is generally used to agitate debris on the ground, which then enters the system through the head, passes through the duct, and ideally settles out into the storage bin. The air continues its path through the filters and the fans. Any debris that doesn't settle out in the storage bin may stay in the airflow and then be separated by the filters.

The functional requirements for the overall robot are outlined below.

Functional Requirements

At the beginning of the project the team composed of Benjamin Schilling, Jody Fu, Youngjun Joh, and Barbara Lima outlined a few functional requirements for the final product that should be generated. These functional requirements also help the final product to set itself apart from the existing products by accounting for some of the areas where they were lacking for application in automated warehouse environments. These are outlined below.

- Retrofit one of the many existing warehouse carrier robots for the cleaning robot vacuum
- Fit within the existing carrier robot's size to ensure that it can navigate the warehouse in a similar manner
- Use the pre-existing power supply used by the current carrier robot to power the fans and brushes
- Ensure that the noise level is 90 decibels or below. This complies with OSHA standards for a normal work day. OSHA states that the permissible exposure limit for noise exposure is 90 decibels for an 8-hour time-weighted average[8]

- Design the holding bin so that it is easy to use and can be emptied in less than 5 minutes
    - Ideally, the cleaning robot would dock and get emptied without human interaction
- Run time: One hour before needing to be recharged
- Able to pick up, at a minimum, cardboard and cement dust
    - Ideally, can pick up liquids and screws along with dust
- Clean over as much as possible of the area the cleaning robot takes up, especially the area where the traction wheels of the carrier robots travel
    - This should be done while also minimizing damage to the floors or any markings on the floor that may be used for navigation

Head Design

In this thesis the focus will be on optimizing the design of the cleaning robot's vacuum head and duct. Some attention will also be given to the brush design since this will fit into the head and affect the flow in that area. The vacuum head is the section where anything entering the system first passes through. It is usually an extended, oblong shape such that it can cover a wider area than the duct when the vacuum is moved. The duct is the section that connects the vacuum head to the debris storage bin. On commercial vacuums for home applications, the duct usually consists of a ribbed, flexible hose and is small in diameter compared to the width of the head. Figure 1 below shows the general appearance of the initial head and duct design before any of the dimensions were adjusted for better airflow. The brush usually rotates partially within the area of the head and has a nominal interference with the area being cleaned so that it can stir up dust.

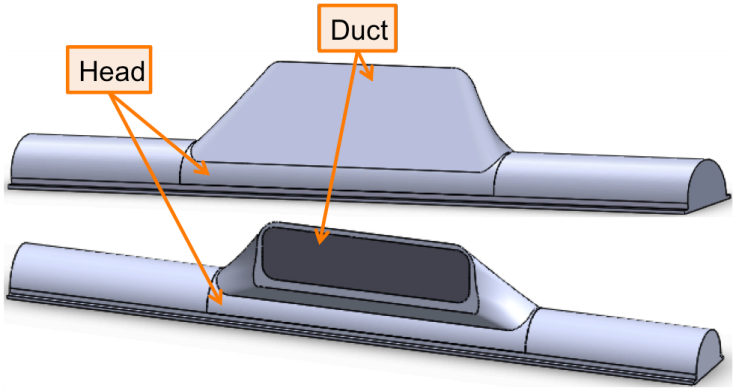

FIGURE 1: INITIAL HEAD DESIGN BEFORE GEOMETRIC OPTIMIZATION.

In order to optimize the design of the head and duct, a range of possible geometries and dimensions for were modeled and computational fluid dynamics (CFD) simulations were carried out. A prototype was then built and tested and lessons learned were applied to the design plans for a second prototype. CFD studies were the main method for initial optimization and the objectives used to compare the different geometries are outlined below.

Head, Duct & Brush Design Objectives

Design objectives for these parts have been drawn up based on the overall functional requirements but with more focus on these three parts.

- Maximize air flow at the entrance to the vacuum head so as to allow for efficient pickup of debris
    - Ensure sufficient air flow throughout the entrance to the vacuum head
    - Distribute air flow as evenly as possible so as to improve efficiency
- Maintain air flow in the duct to move debris into the storage bin
- Use brush to improve debris pickup and especially pickup of small objects

CHAPTER 2: THEORETICAL REVIEW OF CONCEPTS

Vacuum Cleaner Mechanics

Most modern vacuum cleaners function by using vacuum fans to create a low static pressure inside the vacuum that is propagated through the device and generates airflow that can carry debris through the system and into a storage area where it is prevented from exiting until the storage is emptied. The airflow is often not sufficient to lift stationary debris on its own so a brush is used to initially stir up the debris, imparting some initial kinetic energy and allowing for airflow to pass underneath the debris to lift it into the system. The direction of rotation of the brush varies but it is generally preferred to rotate the brush towards the side of the head/duct that has a smoother path into the bin. For the purpose of this project this direction is towards the front of the robot.

In order to store the debris inside the temporary storage bin and not have it all blow out through the other side of the fans or damage the fans, it is necessary to separate the debris from the airflow. This also needs to be carried out in the bin where the debris will be stored as it is difficult to transport the debris again once it has settled out of the airflow. Two main methods used for this debris separation are filters and inertial separation. Filters can be chosen so as to prevent 100% of particles of a minimum size and above passing through the system and getting expelled back into the environment. They do, however, often get clogged and add significant impedance to the system, decreasing the airflow. Vacuums that rely on inertial separation usually require a long design period with extensive fluid flow studies that eventually yield an efficient inertial separation method. Most vacuums that use inertial separation also contain a filter as a backup mechanism but often times the filter is indeed unnecessary in such cases. For the time frame of this project the filter option was chosen as the main mode of separation of the debris and airflow. Benjamin Schilling's thesis deals more in the area of debris and airflow separation as well as storage bin and filter design [9].

Solidworks Computational Fluid Dynamics (CFD) Simulation

Fluid Equations and Methods

The use of Solidworks CFD Simulation in this project was limited to fluid regions and although Solidworks can also solve the associated heat transfer problems within both the fluid and solid regions, these calculations are done separately from the flow calculations and were not taken advantage of for this study [10]. For the main fluid region Solidworks starts with the Navier-Stokes equations and solves these during the simulation [10]. Since this study's main fluid was air, which is compressible, the simulation also uses the energy balance shown in Equation 1 below.

Equation 1: Solidworks's energy balance for high speed flows and flows with shockwaves. Reproduced from Sobachkin 2014[10]

$$\frac{\partial \rho E}{\partial t} + \frac{\partial \rho u_i \left(E + \frac{p}{\rho}\right)}{\partial x_i} = \frac{\partial}{dx_i}\left(u_j\left(\tau_{ij} + \tau_{ij}^R\right) + q_i\right) - \tau_{ij}^R \frac{\partial u_i}{\partial x_i} + \rho\varepsilon + S_i u_i + Q_H$$

$$E = e + \frac{u^2}{2}$$

The Solidworks simulations also draw on other fluid properties and are valid for both laminar and turbulent flow with the transition between the two being smooth [10]. Turbulent flows are calculated using the Favre-averaged Navier-Stokes equations and Solidworks uses the κ-ε model to calculate the dissipation of turbulent energy and complete the set of fully defining system equations [10]. Lam and Bremhost's damping functions are also used in special cases where the Reynolds number is otherwise too small to calculate good heat dissipation [10].

Boundary layers are dealt with via the Prandtl approach in order to compensate for the coarseness of meshing and the Two-Scale Wall Function couples the boundary layer flows to the bulk flow [10].

Numerical Methods

According to Sobachkin 2014 the main numerical methods solver in Solidworks uses "time-implicit approximations of the continuity and convection/diffusion equations" paired together with "an operator-splitting technique" to decouple velocity and pressure [10]. For the resulting asymmetric systems of equations, Solidworks uses the "preconditioned generalized conjugate gradient method from Saad"[11] with LU factorization for preconditioning [10]. For the symmetric systems of equations Solidworks has a unique numerical method based on a multi-grid method [12]. This unique method operates as a "double preconditioned iterative procedure" [10].

CHAPTER 3: METHODOLOGY

In order to decrease the number of iterative design steps and achieve a more advanced design within the time period of the project, initial design optimization was carried out based on CFD simulations carried out in Solidworks. The first prototype was therefore built after several iterations had been tested through the simulations. Measurements of the prototype or taken to determine the accuracy of the initial simulations by comparing the predicted performance with the physical measurements.

Base Design

First Prototype

An initial design for the cleaning robot was developed in CAD using Solidworks to serve as the starting point for CFD-based optimization. The initial design incorporated all the main components needed to add the vacuum function to the existing robot and these were moved around and changed as the project progressed. Figure 2 below shows the CAD for the first prototype with all the main vacuum components. In order to show these components more clearly, most of the other components that serve for general robot function but do not directly impact the vacuum function have been removed. The main vacuum components are the head, brush, duct, debris storage bin, filters, fans, and the brush motor. These are all pictured in Figure 2 below but the brush can only be seen from the bottom view since it sits inside the head. The fans create a lower static pressure inside the bin than outside and this drives the airflow through the entire system. Debris is first stirred up by the brush and then enters the head, passes through the duct and into the bin where most of it should settle out of the airflow stream. Any dust remaining in the airflow stream is caught in the filters just before the air exits the system through the fans. The control center sits in the back half of the chassis and was used in the prototyping stage to allow for the brush motor and fans to be manually turned on and off as well as tuned for speed. In this thesis the focus is on the design of the head, brush, and duct while Benjamin Schilling's thesis focuses on the design and choice of bin, filters, and fans.

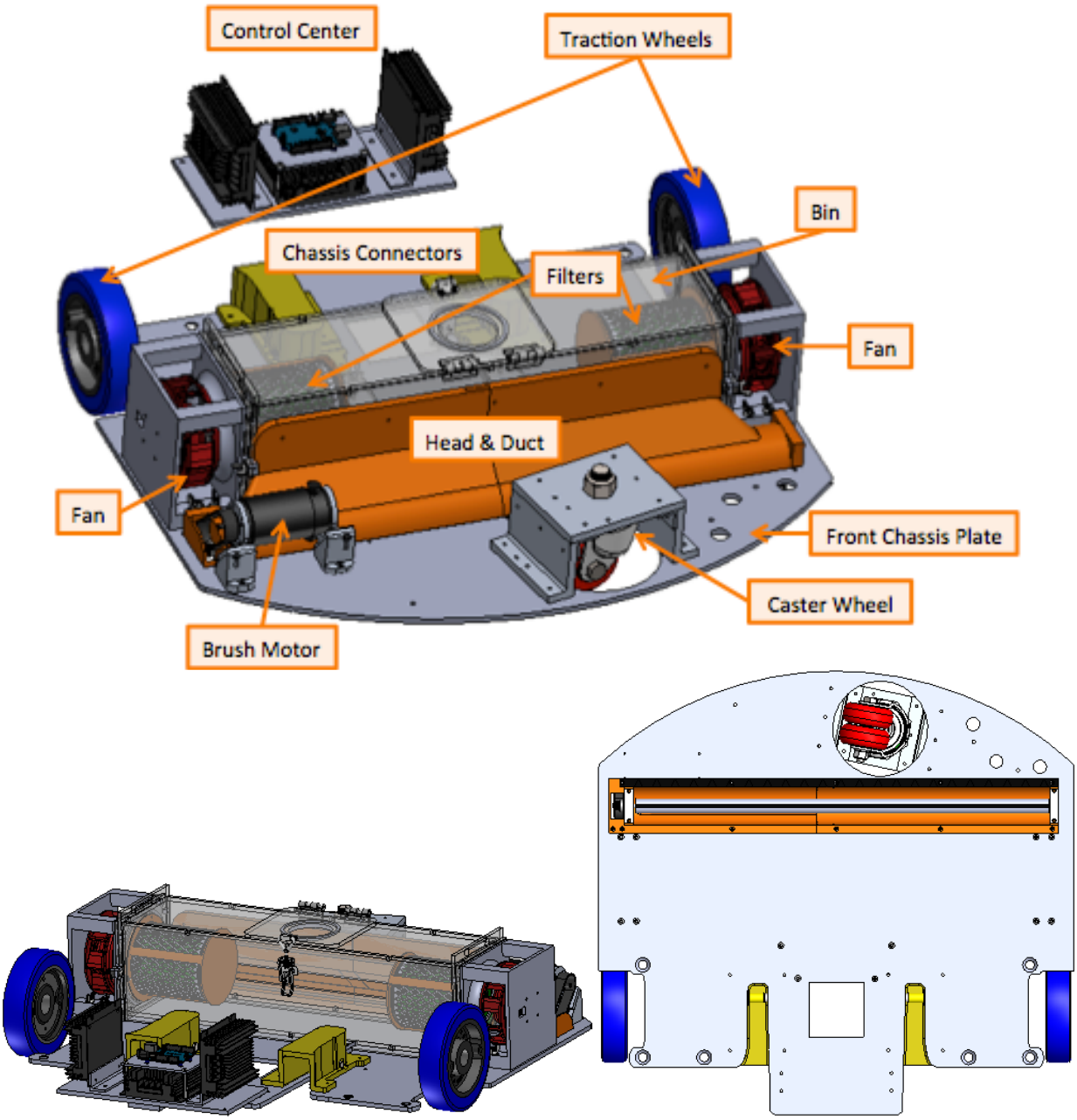

FIGURE 2: OVERVIEW OF CAD FOR FIRST PROTOTYPE

The main components that have been left in the image from non-vacuum functions are the caster wheel, the traction wheels, and the chassis connectors. The caster wheel is weight bearing but does not serve any function in navigation or moving the robot – the traction wheels carry out these functions. The traction wheel path is one of the most important areas to clean because this is where errors can occur that lead to inaccurate navigation. It can be seen that the first prototype did not cover the tracks of the traction wheels

completely. This was due to space constraints and structural strength of the front chassis plate. Lastly, the figure depicts only the front chassis but the full robot also contains a second half of the chassis that is linked to the pictured front via a pin and the yellow connectors shown.

Head & Duct

First Prototype

The head of the vacuum is one of the most crucial components since it significantly influences the airflow and dictates how efficiently the potential for picking up dust is translated between the fans and the entrance to the head where all the debris will be located initially. Since one of the aims of the project is to maximize cleaning, it was decided that the head width would be set near to the width of the robot with just sufficient material left at the sides to provide structural support. Since optimization of the head shape was needed, it was initially modeled as two separate parts to facilitate parameterization. One that was the head base dictating the overall width of the head and adding material to complete any areas left uncovered by the second part, the middle section. The middle section contained all the crucial geometries of the head: the duct for connection to the bin and the cutout in the top of the head for connection to the duct. In optimizing the head, the middle section was changed progressively and CFD simulations were run with it while the head base simply completed any necessary width and brush covering not accounted for in the middle section.

In order to allow for a parameterized head that could be easily changed to study effect on flow, the middle section was designed as two main parts: the cover over the brush and the duct leading to the bin. Most commercial vacuum cleaners currently use a hose that acts as the duct between the main head part and the debris storage bin, but in order to have more design freedom it was planned to have the whole head, including the duct, 3D printed and rigid. This ensured that the duct shape could be changed as freely as the main head part covering the brush. The brush cover was designed as a semicircle with straight edges at the bottom to allow for coupling with the thickness of the chassis plate. The semicircle was extruded over the length of the brush and a cutout was made at the top (centered) to allow

for connection into the duct. Straight edges at the ends of the semicircle were needed for coupling to the thickness of the chassis plate because the head was designed so as to be fit in through the bottom of the chassis and the flanges would attach to the bottom side of the plate as well. This was done to eliminate the creation of a seam between the head and the chassis that would then need to be sealed via O-rings or another method. The duct was designed as a straight path between the cutout in the brush cover and the hole in the bin. This was done to maintain the path as short as possible and therefore decrease the amount of impedance generated. The edges inside corners of the duct were filleted to remove potentially turbulent corners and the duct was designed in such a way that the opening in the brush cover section of the head always had to be wider than the opening in the bin. This was done because it was expected that the opening at the brush cover as well as the head would need to be as wide as possible whereas the opening at the bin was restricted by the bin size. The bin size had to be less than the width of the robot due to the need to mount the fans to each side of the bin.

Extra features were added to the first prototype's brush to create a section for the attachment to the motor's belt and bearing-like parts were 3D printed to insert the brushes into the head from underneath and hold them in place during operation.

Second Prototype

For the second prototype, the head duct was flared out to allow for better airflow and the shape of the brush covering was made into an oval to allow for the brush shaft to sit higher within it but most of the other components were held relatively constant. The number of heads in the second prototype also did change and this brought in a need to make the head more asymmetric. The details of why the given changes were made and how they were carried out are further discussed in the chapter 4.

Brushes

Brushes were initially going to be obtained commercially but after a first iteration showed this was not necessarily better than designing a unique brush, a straight-bristled wooden brush was used for the first prototype and the second prototype had a set of straight-bristled and a set of helical brushes, both of which were 3D printed.

Debris Storage Bin

First Prototype

The first prototype's bin was designed as a rectangular box so as to allow for a quick build using laser-cut acrylic and acrylic glue. The four sides were cut out of acrylic with notches that complemented each other to help with alignment during assembly.

Second Prototype

For the second prototype, the bin was changed to a cylindrical one to improve inertial separation. This is discussed more fully in Benjamin Schilling's thesis [9].

Second Prototype

Several changes were carried out to improve the design on the second prototype. The main changes were that the head was split in two to allow for coverage of the wheel tracks, a specialized duct for fiducial cleaning was added to account for the space between the heads, the bin was made cylindrical, a better blower housing was designed for good airflow and better sealing with the filter and bin, and helical brushes were used. In this thesis the focus will be on discussing the changes carried out to the head, duct, and brush. Figure 3 below shows the top and bottom views of the CAD model for the second prototype.

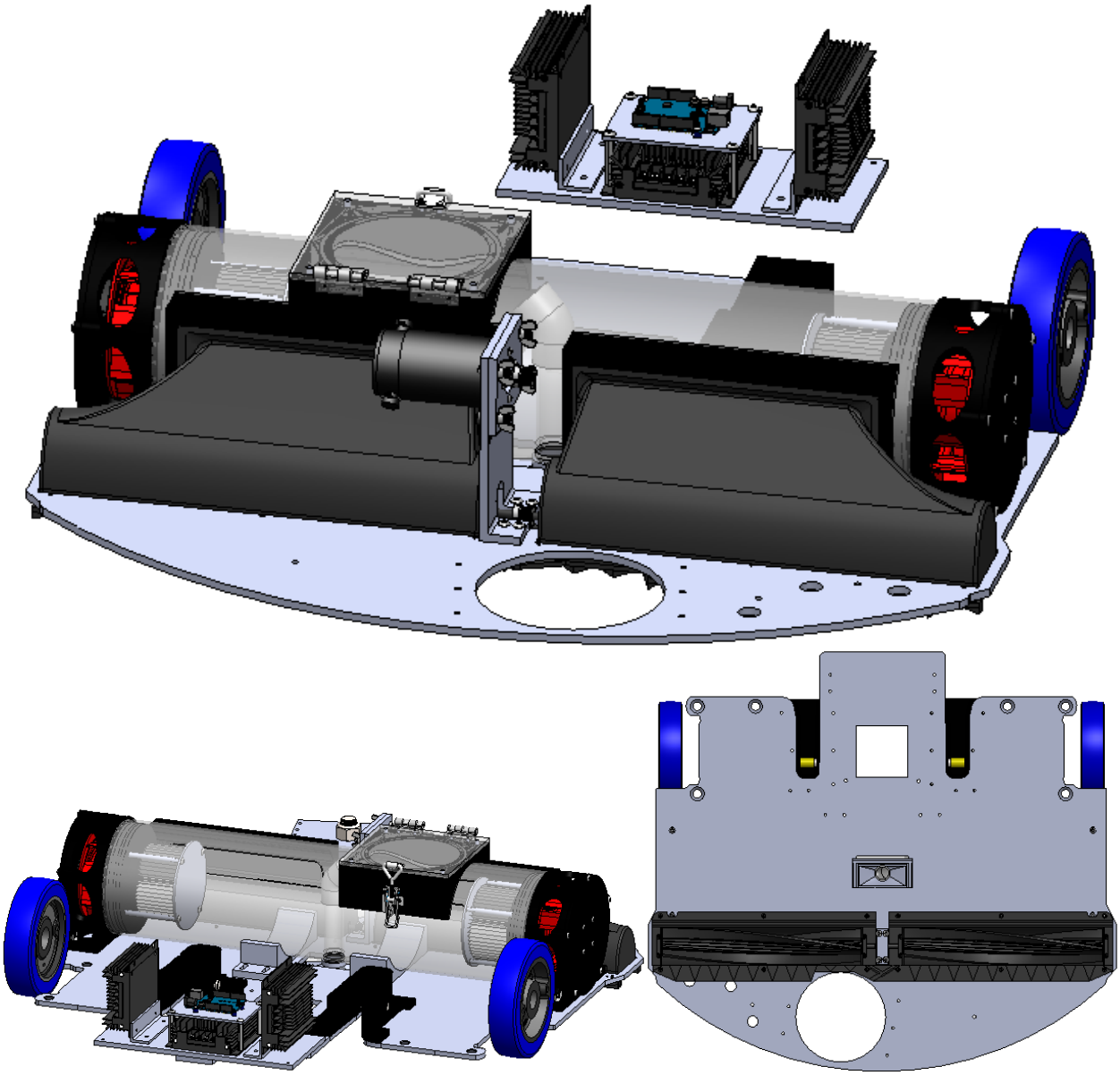

FIGURE 3: OVERVIEW OF CAD FOR SECOND PROTOTYPE. THE FRONT CASTER WHEEL HAS ALSO BEEN REMOVED FROM THIS IMAGE TO ALLOW FOR BETTER VISUALIZATION OF THE BRUSH MOTOR MOUNTING.

CFD Simulations

Inputs & Setup

CFD was carried out using the vacuum head, duct, and bin setup with a simplified brush model. The filters were not modeled into the system as this was deemed unnecessary. The small pore size of the filters would require for the mesh sized to be significantly decreased for accurate calculation and this would lead to impractically long computational times for each simulation. Since there was not sufficient time to accurately calculate flow paths with

the filter in the model it was completely omitted. Losses due to the filter were accounted for by derating the fans. This is discussed below. In addition to adding impedance due to the actual paper filter, the filter also adds impedance due to the outlet diameter for air flow that is smaller than the fans' inlets. This was not considered during optimization but tests with the final first prototype planned design were carried out to test its effect on predicted air flow velocities.

The floor was also added to the model in order to account for restrictions in airflow that occur before the air has even reached the entrance to the vacuum head. Lastly, a rubber scraper was added behind the head as this also helps in directing air from in front into the head and restricting airflow from the back. This allows for higher air velocity into the head. The chassis plate was also included in the model but this was just for aid in positioning of the parts and did not have an effect on the simulation.

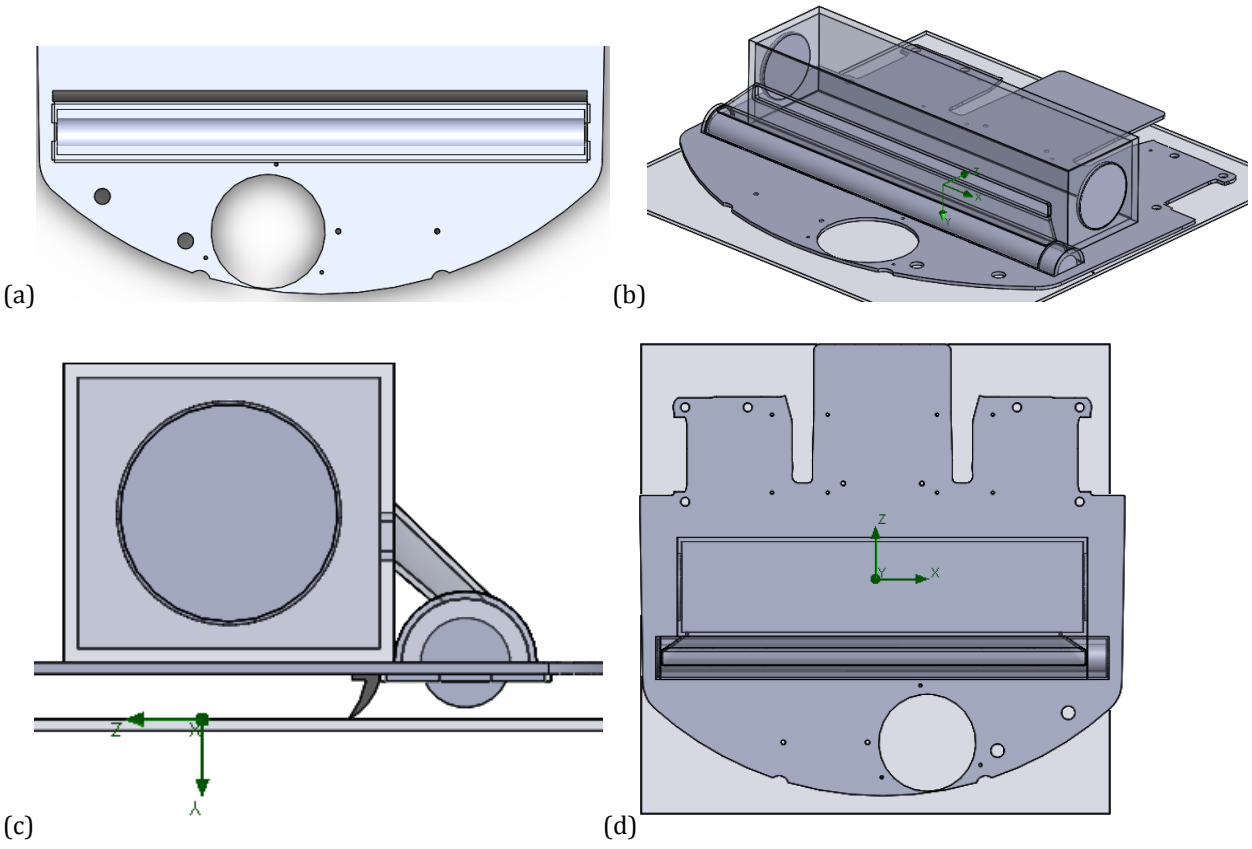

FIGURE 4: SYSTEM MODEL FOR CFD SIMULATION (A) BOTTOM VIEW (B) ISOMETRIC (C) SIDE VIEW (D) TOP VIEW

Fans

The fans were modeled in as user defined fans on the lids directly on the sides of the bin. Since the fans were modeled only on the lids of the bin, the size of the opening in the bin connecting to the fans was taken into account. However, the casing that the fan would eventually be mounted in was not accounted for. By adding the casing some extra resistance to air flow would be added but the overall directionality of increasing or decreasing airflow at the head would not be affected.

Values from the fan curve on the fan specificationss were taken and put into the solidworks simulation as user defined fans. The curves on the spec sheet and the one put into the simulation are shown in Figure 5 a and b below. The fan was defined as an external outlet fan and derated values were used to simulate a dirty filter decreasing airflow. The dirty filter simulation was carried out by halving all the values on the horizontal and vertical values on the fan curve. The derated fan curve is shown in Figure 2c but this was not used for optimization - it was used after simulation was carried out and before prototyping to ensure that sufficient velocity would be achieved even when the filter was dirty.

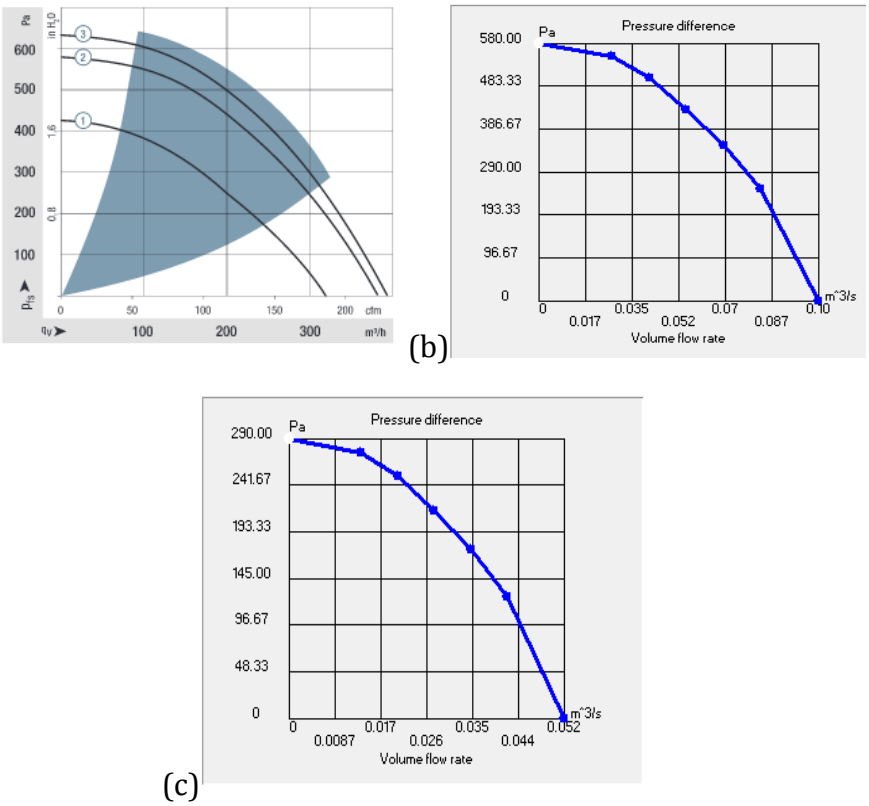

FIGURE 5 (A) FAN CURVE NUMBER 2 FOR THE RER 120-26/14/2 TDP [13](B) FAN CURVE FOR RER 120-26/14/2 TDP USED IN SOLIDWORKS SIMULATION (C) DERATED FAN CURVE USED IN SOLIDWORKS SIMULATION AS A PROXY FOR A DIRTY FILTER

Brush

A simplified model was used for the brush because during the initial studies the full brush dimensions were not yet known since the parts had not yet arrived. The bristles of the brush would again add too much complexity to the system and the detail was therefore left out. During operation the brush would be rotating and the bristles would therefore be blocking airflow at one point or another inside the head, so the brush was modeled as a solid cylinder with the expected diameter of the ordered brushes plus their bristles. For first prototype simulations the brush rotation was therefore accounted for simply by blocking off its whole area of operation and contributions to airflow made by the brush were not accounted for. It was expected that this contribution would be small. Even if the brush rotation had a significant contribution, however, it could still be ignored in the first prototype's simulations. This was justified because the brush would rotate in a single direction and any contribution made to airflow in the head to one side of the brush would

be equal but opposite to its contribution on the other side of the brush so these two effects could be considered to approximately cancel out.

Bin

The debris storage bin was modeled as a simple rectangular box with cutouts incorporated for the connection to each of the fans and to the head. The cutouts for the fans were the correct size according to the recommendation for the fans that were purchased and cutout for the head connection was also equivalent to the size of the opening at the end of the duct.

Head

For CFD, many of the features of the head and duct were maintained as true as possible to what was expected in the final prototype. This is because the head and duct geometries were major determinants in the simulation results. The internal shapes of the duct and head were therefore maintained with only some of the features made for mechanical attachment to other parts - such as the flanges for attachment to the bin, and the mounts for the brush - removed. Figure 6 below shows the CAD model used to run CFD how it stood near the end of the optimization process.

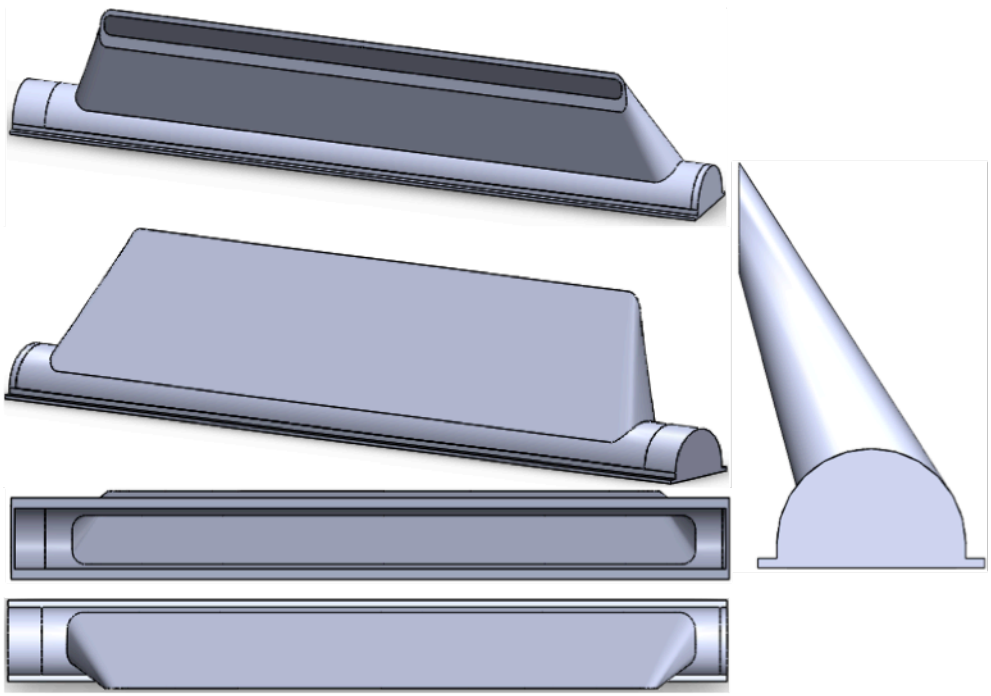

FIGURE 6: CAD OF BASIC HEAD GEOMETRY

Boundary Conditions and Meshing

The boundary condition at the head entrance lid was set to atmospheric pressure and the global mesh was set at a level 3 with localized meshing at the head, duct, and brush area adding 2 refinement cells for fluid and solid-fluid boundaries.

Design of Experiments

In order to optimize the head shape, it was first necessary to pick which variables could be changed to yield these different geometries. The variables chosen are listed in Table 2 below and Figure 7 shows them on the head design. The variables have each been given a letter code so as to better show them in equation form later on. The minimum and maximum value constraints are due to the geometric restrictions of how the different parts of the model fit together and how the head fits with the rest of the drive. Some of the restrictions, such as minimum duct-to-bin opening width are set as practical limits below which it is not believed to be relevant to explore for the purpose of this study. These variables were set as the input variables in a Solidworks Design of Experiments and Optimization Parametric Study along with their ranges that are listed. In addition to this, there were also additional constraints due to geometry that dictated that $A < E$, $B > 2C$, and $D + B \leq 5$ in. must all be true. The initial data collected was therefore not a proper full factorial study since accommodations had to be made for these additional constraints. To accommodate for these constraints, any original full factorial design points that did not naturally fit into the constraints were adjusted according to the following rules and for the following reasons:

- If $A < E$ is not true, increase E as it is expected that wider openings will be better for airflow
- If $B > 2C$ is not true, decrease C as fillet sizes are not expected to have a large impact
- If $D + B \leq 5$ in is not true, decrease D as this will keep the duct-to-bin connection at the very top of the bin

Table 2: CFD optimization input factors

Factor Code	Description	Low (in)	High (in)
A	Duct-to-Bin Opening Width	4	20
B	Duct-to-Bin Opening Height	0.75	2
C	Duct-to-Bin Opening Fillet	0.25	0.5
D	Duct-to-Bin Opening Elevation (Location on Bin)	1.5	4.25
E	Head-to-Duct Opening Width	6	23
F	Head-to-Duct Opening Height	1.3	2

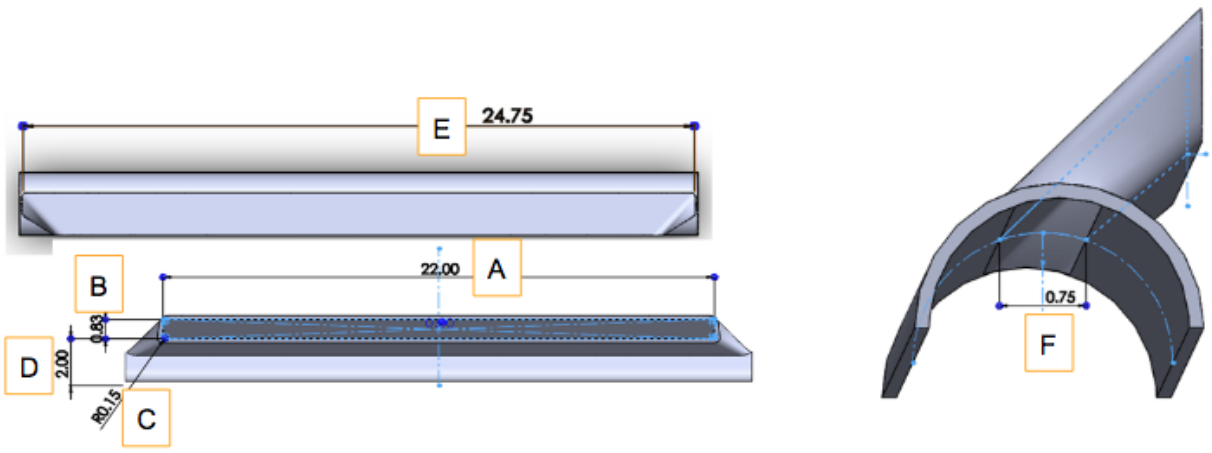

FIGURE 7: VISUALIZATION OF CFD OPTIMIZATION INPUT FACTORS

Due to the interdependence of the variables, several ranges were tested for the variables with the initial range set very liberally. Even by accounting for the more obvious additional constraints mentioned above, some of the generated scenarios were not able to run successfully in the simulation and this is what motivated the use of subsequently more conservative ranges for each of the variables. Table 3 below shows the two sets of ranges that were used before arriving at the one shown in Table 2 above. On the third iteration of ranges some simulation scenarios still failed to run but by this iteration 105 unique scenarios had already been run (taking into consideration all the previous experiments with the previous ranges) and it was determined these results were sufficient as an initial set. Given that 6 factors were being considered, a full factorial would require 64 unique experiments and this had therefore been more than satisfied. Since the geometry was being changed in each experiment, each simulation had to be remeshed and then run – each simulation took on the order of a few minutes to run.

Table 3: Initial variable ranges based on intuitive geometric restrictions imposed by other components and the first round of iteration to a more conservative set of ranges before moving to the final range shown in Table 2. The * indicates values that were changed over the course of iterations.

Original Iteration

Factor Code	Description	Low (in)	High (in)
A	Duct-to-Bin Opening Width	2*	22*
B	Duct-to-Bin Opening Height	0.75	2
C	Duct-to-Bin Opening Fillet	0.05*	0.5
D	Duct-to-Bin Opening Elevation (Location on Bin)	0.5*	4.35*
E	Head-to-Duct Opening Width	2.5*	24.75*
F	Head-to-Duct Opening Height	1.3	2.2*

First Round Iteration

Factor Code	Description	Low (in)	High (in)
A	Duct-to-Bin Opening Width	4*	22*
B	Duct-to-Bin Opening Height	0.75	2
C	Duct-to-Bin Opening Fillet	0.25*	0.5
D	Duct-to-Bin Opening Elevation (Location on Bin)	1.5*	4.35*
E	Head-to-Duct Opening Width	6*	24.75*
F	Head-to-Duct Opening Height	1.3	2.2*

The output variable was the minimum velocity across the head entrance. Four point measurements were also made along the head entrance towards the outsides but these are not necessarily the minimum velocities and were used simply for double checking results. The goal was to maximize the output factor of minimum velocity.

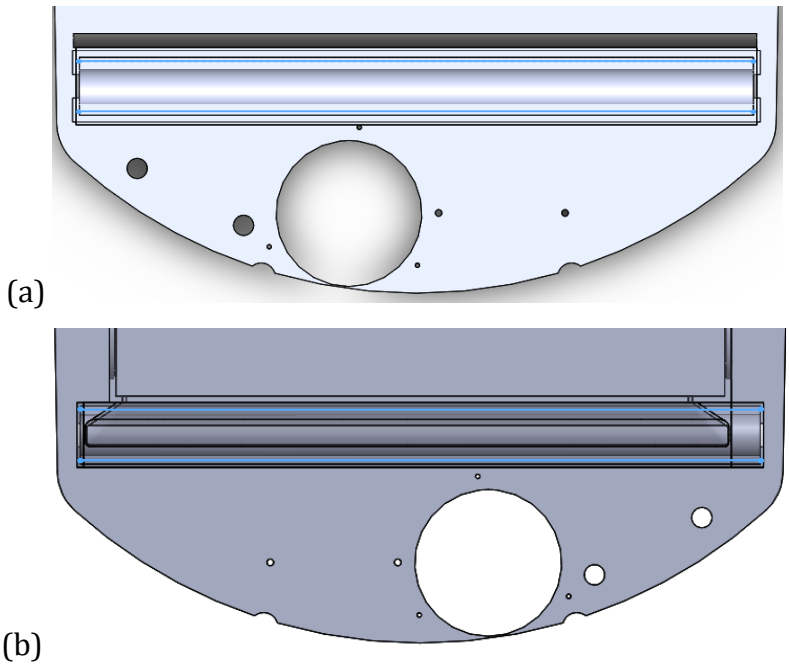

FIGURE 8: THE TWO BLUE LINES ON THE DIAGRAM INDICATE THE AREA WHERE THE VELOCITY AT THE HEAD ENTRANCE WAS MEASURED AND FROM WHICH THE MINIMUM VELOCITY AT THE HEAD WAS SELECTED. (A) SHOWS THE VIEW FROM THE BOTTOM OF THE ROBOT AND (B) SHOWS THE VIEW FROM THE TOP OF THE ROBOT

Optimization

Optimization was carried out by first taking results from several CFD simulations and then using these to build a model based on all the factors. The model was then used to determine the optimum values for all the input factors.

The metric chosen as the optimization variable was the minimum velocity at the head's entrance. This was chosen because if the minimum velocity at the head's entrance is maximized, then it is pretty much ensured that velocity everywhere else in the head and duct will be higher and therefore more capable of picking up dust. By improving the weakest point, the best geometry can therefore be determined. Looking at the complete system, the real goal is to have the velocity distribution be as uniform as possible because this decreases the chances of dust dropping out of the airflow along the path in the head or duct and also improves efficiency of the system overall. If the velocity is not evenly distributed then the fans must be strong enough so that even the lowest velocity can still pick up the debris, which means that most other areas have excessive velocity and represent efficiency losses since more than the required energy is being used. By looking

only at the minimum velocity at the head entrance and keeping the fans and bin constant, however, the overall desired effect can still be achieved since most increases in this minimum velocity mean that either the whole system's velocity is increasing too or potential from other higher velocity areas is being reassigned to boost the minimum velocity.

Minitab was used to analyze all the data acquired through the CFD simulations and build a model through linear regression. Since there was sufficient data to include all possible factors and since the data was not from physical experiments but rather from simulations, all the factors were left in the model and none were omitted. This included squared terms.

The optimization was carried out by building a model independently and not by using the optimization function in the Solidworks study because the additional geometric constraints (other than the variable ranges) could not be input into the study. This caused most of the movement towards an optimum to move into areas where geometries were invalid and the simulations therefore failed. By building a model and optimizing the model's output in Matlab and by steepest ascent the extra geometric constraints were accounted for and final results were double checked through the simulation. Optimization was carried out through three different methods that all lead to the same result.

A manual steepest ascent method was done in Excel by moving 1/10,000 units in the direction of steepest ascent until movement in that direction was no longer within the acceptable range for each variable. This was done by moving each variable by the product of 1/10,000 and the derivative with respect to the given variable at the current location. Each time a variable needed to move beyond the limit of its range it was instead brought back to that max/min value so that other variables could continue to be optimized. The steps for optimization are shown in Appendix A.

Matlab's "fmincon" function was also used on the model to check the manual steepest ascent optimization. The default "interior-point" algorithm was used and the function was subsequently also run with the "sqp" algorithm.

Build Phase

During the build phase for the first prototype some final adjustments were made to parts as they were fitted together. The part files were kept as updated as possible with the latest changes so that a last CFD simulation could be run using the final form of the prototype before comparing the simulation results with the physical measurements.

Prototype Measurements & CFD Accuracy Confirmation

Performance Testing

Vacuum performance was also measured by running tests on how much debris the robot could pick up. These were carried out by spreading a controlled mass of flour on the ground over a set distance in the robot's path and then having the robot drive over this with the vacuum turned on. During the experiments carried out here the robot was traveling at approximately 1.5 m/s over the debris area. The flour was spread in such a way that it was not located in the area where the robot started or ended its run such that it would not idle over any area where the flour had been originally set down. The storage bin was then emptied out using another small vacuum and the flour collected from inside the bin was weighed. The experiments were carried out at different settings for the fan and brush speeds and results were analyzed for impact of these factors and for performance of the vacuum.

Velocity Measurements

After the prototype was fully assembled velocity measurements were taken at the exit of the duct into the bin using an Extech Mini Thermo-Anemometer and a final CFD simulation was carried out using the most up to date model of part dimensions and positioning. The measurements were used to compare against the predictions of the CFD simulation in order to validate the accuracy of the simulations that had been used to optimize the design in the first place.

For the velocity measurements, the probe was positioned as in Figure 9 below so as to measure the velocity of air in the direction parallel to the ground and perpendicular to the sidewall of the bin through which it was entering.

FIGURE 9: SETUP FOR VELOCITY MEASUREMENTS OF AIR EXITING THE HEAD DUCT

The velocity measurements were taken at three locations on the duct exit: the center of the duct and to the right and left of center at the point where the cylindrical filters were no longer in front of the duct.

Chapter 4: Analysis

First Prototype's CFD Optimization

Number of Heads

During the design process, consideration was given to the possibility of having multiple heads attached to the same or separate bins. In Benjamin Schilling's thesis the choice of using two fans is discussed and this lead to the possibility of having one or two separate bins which could attach to one or multiple heads.

It was decided that the one-headed design would be a better option for the first prototype. By having multiple heads, the optimized cleaning area could be moved outwards towards the wheel paths but the overall quality of cleaning would be decreased because the number of lower velocity edges would be doubled. Since the first prototype would be mainly a proof of concept, the main goal was to build a vacuum that could pick up the intended debris. By maintaining a single head, the vacuum performance could be maintained a little higher for the proof of concept before a more useful vacuum for cleaning wheel paths was developed. The two heads with two ducts created more stagnated areas since chassis space had to be maintained on the outsides of the robot and another space would be added in the middle. The space on the outsides of the robot are needed for structural stability and that in the middle would be needed to separate the two heads from each other in order to drive both heads with a single motor. As mentioned, the loss of this area from the vacuum head to inactive area causes the overall quality of cleaning to decrease since there will be more area that is not cleaned as efficiently. In addition to losing area directly there are also more corners and edges introduced into the system where there will still be airflow but it will be weak. The benefits of splitting the head space into two, are that it might be possible to move them further towards the outsides to clean the wheelpaths and by splitting the ducts as well, it is possible to avoid some of the eddies and unevenness generated in the center of the wide duct. The overall effect can be seen in the CFD Simulation results shown in Figure 10 below. Ultimately it was decided that for the first proof-of-concept prototype the

priority was in ensuring that the vacuum was able to pick up debris appropriately and the one-headed design was chosen to maximize the chances of this.

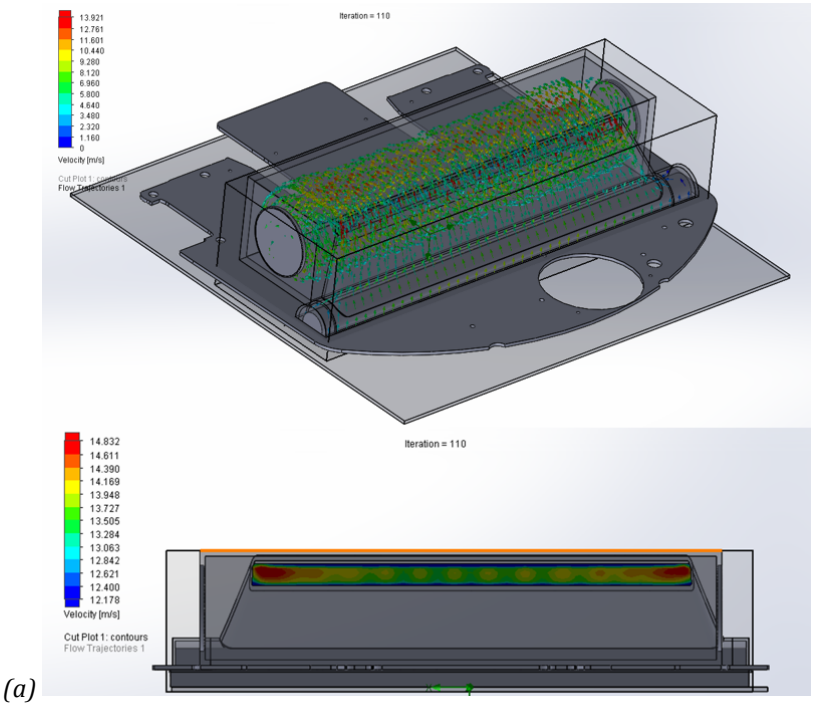

(a)

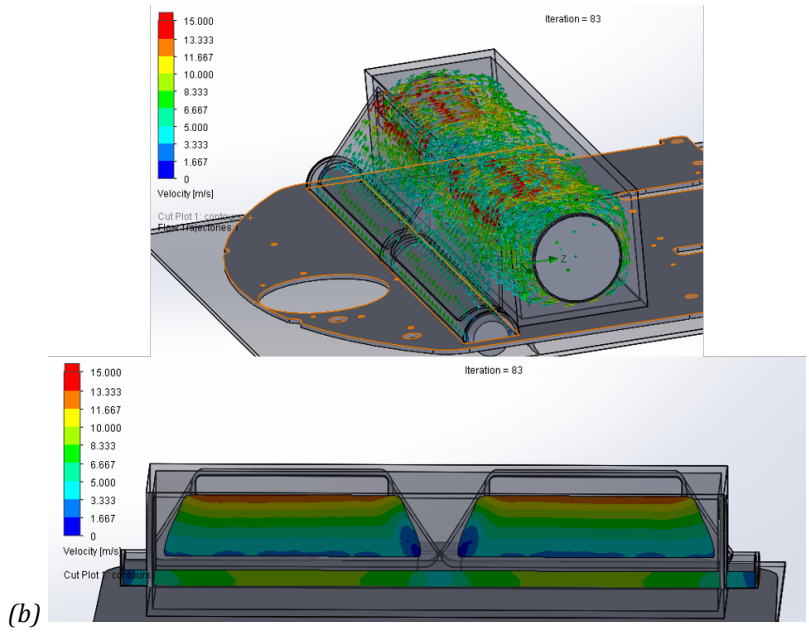

(b)

FIGURE 10: COMPARISON OF (A) ONE-HEADED AND (B) TWO-HEADED HEAD DESIGNS WITH THE SAME FAN SETTINS AND SIMILAR HEAD PARAMETERS. THE HEAD PARAMETERS FOR THE ONE-HEADED DESIGN ARE AS FOLLOWS: DUCT TOP DIMENSIONS = 20"W (A) X 0.75"H (B), ELEVATION = 4.25" (D), DUCT BOTTOM DIMENSIONS: 23"W (E) X 1.8"H (F) AND FILLET R = 0.15" (C) ROLLER DIAMETER: 1.57". THE HEAD

PARAMETERS FOR THE TW-HEADED DESIGN ARE AS FOLLOWS: DUCT TOP DIMENSIONS (X2): 8"W (A) X 1"H (B) AND FILLET R = 0.5" (C), ELEVATION: 4" (D), DUCT BOTTOM DIMENSIONS: 12"W (E) X 1.8"H (F), ROLLER DIAMETER: 1.57".

Once testing of the first prototype's performance was complete it became evident that the design was sufficiently capable of picking up debris on first and second passes at its current state. This allowed for more exploration into the two-headed design for the second prototype since the initial tests had been carried out at the robot's maximum speed and it could be slowed down if needed to improve first-pass pickup rate of a two-headed design. This way it would be possible to take advantage of the benefits of the two-headed design while still achieving acceptable debris pickup. In the second prototype the two-headed design was coupled with a center brush and center duct for eliminating the unreachable zone between the two ducts. The optimization carried out for the head in the first prototype, however, yielded trends that are useful for both the one-headed and two-headed designs since each duct can still be looked at as a single unit in the two-headed design.

In order to accommodate the two heads in the second prototype and extend them to clean the wheel path it was necessary to extend the chassis slightly past the first prototype robot dimensions. In a warehouse where space is restricted and used to the maximum to cut costs and increase efficiency, this could be problematic. In a final production scale version of the two-headed robot the front chassis would therefore no longer be a flat plate but would be taken into a 3D shape such that there would no longer be a necessity to have extra structural material on the outsides of the heads since it could instead be replaced with structural material that sits over the head. For the purposes of second testing, extending the width of the robot did not pose any serious problems and this solution was adopted since it was easier and faster to build, allowing for the main chassis to be created using a waterjet. The 3-dimensional solution would later be created by adding extra parts that connect to the main chassis or by having a cast or fully machined chassis.

Additionally, the motor and belt for the brush in the head that were originally located to one side of the head in the first prototype were moved to the center into the space between the two heads. For structural purposes of the prototype it was necessary to keep as much material as possible where the chassis could connect around the heads. The axis of the brush was therefore brought to above the chassis plate in order to avoid the need for having an opening in the plate to allow for the connection between the brush motor and the brush shaft. Ultimately both brushes were being driven by the same motor through a shaft that connected the two brushes so it was necessary to have an opening through which the shaft could pass through during assembly since the head was mounted from the bottom. This hole was, however, be closed once assembly was complete by adding a supporting plate to the bottom of the chassis and bridging the gap. This would not be the case if a hole needed to be left for a belt to run between the brush motor and the brush shaft.

Choosing the Best Head & Duct Shape

The CFD simulation results collected in the first stage of optimization are shown in Appendix B. When a model was fitted to these results, the relationships found between the input factors and the minimum velocity at the head entrance were those shown in Equation 2 below. Figure 11 shows that although there appears to be some abnormality in the residuals plot, the distribution seems to be normal for the most part.

Equation 2: Velocity relationship to the head parameters

$$\begin{aligned} Velocity\ \left(\frac{m}{s}\right) = {} & 29.8 - 24.02\,A - 1581\,B - 349\,C + 104.2\,D + 5.47\,E - 393\,F \\ & - 4.77\,A^2 + 22302\,B^2 + 5498\,C^2 - 678\,D^2 - 13.3\,E^2 + 4258\,F^2 \\ & + 56.3\,AB - 157.7\,AC - 12.2\,AD + 52.0\,AE - 33.7\,AF + 3253\,BC \\ & - 705\,BD + 4.3\,BE + 526\,BF + 538\,CD - 29\,CE + 3544\,CF + 5.5\,DE \\ & - 13\,DF - 14.7\,EF \end{aligned}$$

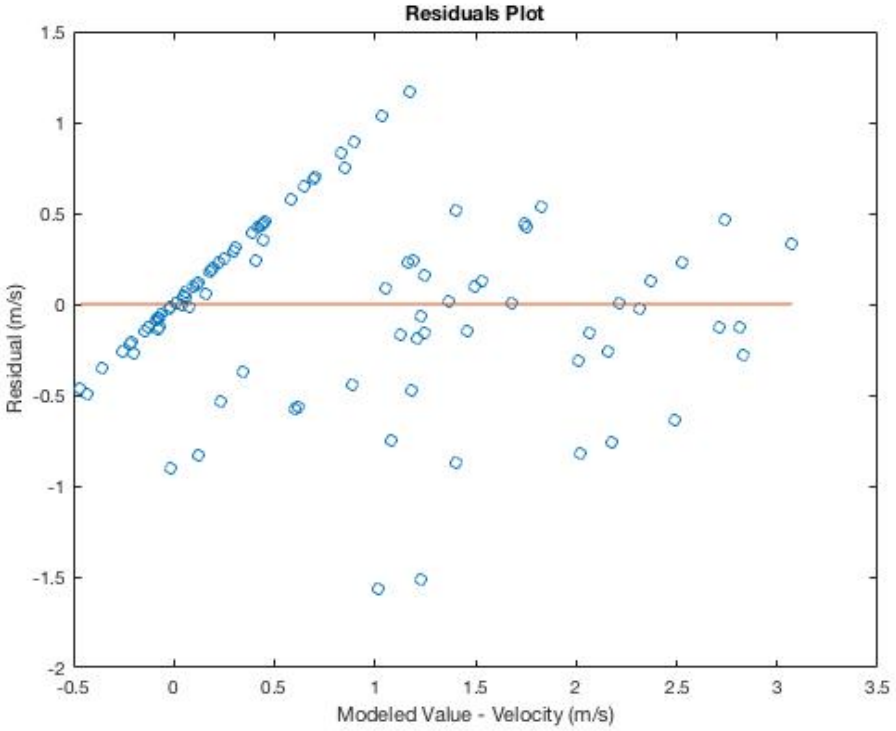

FIGURE 11: RESIDUAL PLOT OF VELOCITY MODEL AND CFD DATA

By steepest ascent and the "interior-point" and "sqp" algorithms in Matlab's "fmincon" function, it was found that the minimum velocity at the head entrance is maximized by maximizing all of the factors except the elevation of the duct (D). The steepest ascent method and each step taken are shown in Appendix A.

It was noticed that increasing variable F, the head to duct opening height, significantly changed the overall geometric design of the head and essentially created a head that was mostly just duct. This suggested that a more flared design of the duct should be explored such that the duct and head incorporated better as a single part rather than having a duct that came off the rectangular cutout in the head. Having the duct connect directly to the brush covering section of the head and considering both parts mostly separately and not necessarily their joint, created a sharp transition between the airflow in the head and that in the duct. The sudden reduction in the size of the volume where air can flow in the head to that in the duct creates a head loss that decreases the airflow especially towards the outer edges of the head where the duct has no direct connection. The outer edges are

therefore left as more stagnant areas as the air rushes in mostly through the same cross sectional area where it can continue more directly into the duct.

The difference in impedance generated by a sharp and flared duct can be grasped by looking at the velocity heads lost by each geometry. The relationships are different for laminar and turbulent flow[14]. At a kinematic viscosity between 15.11-16.97 x 10^{-6} m^2/s (20˚C-40˚C), the flow of air in the duct is almost certainly going to be turbulent or in the laminar-turbulent transition area. Since the duct starts off having the dimensions of the cutout at the head, its characteristic dimension is 1.45 in or approximately 0.4m. In order to maintain laminar flow under these conditions the velocity of the air entering the duct would have to be 0.94m/s - 1.06m/s depending on the temperature. Most of the CFD simulations carried out show velocities well above this inside the duct and even under the worst conditions the velocity tended to be around 1m/s at the head entrance and higher by the time it got to the duct.

For turbulent flows, the velocity head loss is given by the relationship shown in Equation 3 below[14]. For the first prototype head this means a loss of about 0.34 velocity heads. Meanwhile, for a more "trumpet-shaped," rounded shaped contraction with a radius greater than or equal to 15% of the outgoing pipe diameter (or characteristic length), the velocity head loss is only 0.1[14]. This is due in large part to the elimination of the vena contracta when the head is rounded[14]. The rounding of the duct could therefore help decrease the head loss to approximately 30% of its initial state in the first prototype head.

Equation 3: velocity head loss through a sudden contraction for turbulent flows[14]

$$K = 0.5(1 - \frac{A_2}{A_1})$$

Since there was not sufficient time to completely change the head geometry before the first prototype and actually using the maximum dimension for the F variable would create significant interference between the duct and the brush, a smaller value was used for F. Instead of being maximized, F was chosen so as to maintain the same cross sectional area

open to airflow that was present at the head's entrance. This would allow for a more uniform velocity distribution not only within each cross section, but also throughout the head, and duct. Since the F factor was no longer maximized, this meant that the duct-to-bin opening height (B) was also decreased so as to again maintain the same cross sectional area. The final dimensions for the first prototype head are shown in Table 4 below and the final design is shown in Figure 12.

Table 4: values used for factors in first prototype head

Factor Code	Description	First Prototype Value (in)
A	Duct-to-Bin Opening Width	20
B	Duct-to-Bin Opening Height	0.91
C	Duct-to-Bin Opening Fillet	0.15
D	Duct-to-Bin Opening Elevation (Location on Bin)	2
E	Head-to-Duct Opening Width	23.5
F	Head-to-Duct Opening Height	0.75

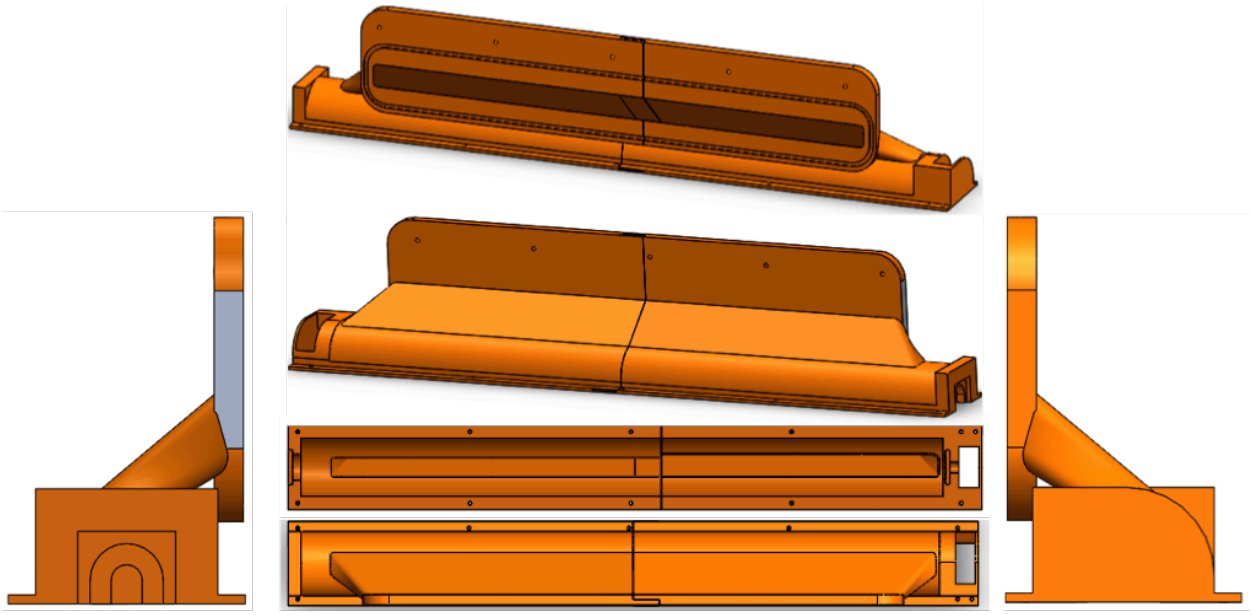

FIGURE 12: FIRST PROTOTYPE HEAD

In the second iteration of the prototype the brush axis was lifted and a change to the head shape was required in order to accommodate for this. If the original semicircular brush cover section of the head was maintained, it would have been necessary to significantly increase the radius of the semicircle in order to avoid interference between the lifted brush and the head. By simply increasing the diameter of the head however, the cross-sectional

area around the brush would become vey uneven and the vacuum head would be made to take up an unnecessarily large quantity of space on the chassis. This extra space could be more useful in other parts of the vacuum, such as in the debris storage bin. To maintain a more constant cross-sectional area and a relatively small space usage, the head was therefore redesigned so as to have an elliptical covering with the same extra straight edge at the bottom for fitting with the thickness of the chassis plate. The elliptical shape allowed for the brush to be mounted higher without interference. It is important that even interference with the brush bristles is avoided as this would add extra resistance to the movement of the brush and would therefore slow down the rotation. This is undesirable since it would decrease the efficiency with which the brush pushes debris and larger objects into the head and agitates the dust so that it can be carried into the head by the airflow. In addition to creating the more elliptical head for the raised brush, the results from the head shape optimization were fully considered and the duct was designed to follow a concave up (up being the direction towards the bin) curvature between the debris storage bin connection and the connection to the head. Since the heads were moved towards the outsides of the robot this was also useful because the each head now needed to be asymmetric and a mirror copy of the other in order to reach both the edge of the robot and the bin while maintaining as wide a duct as possible. The final dimensions for the second prototype head and an image of the head CAD are shown in Table 5 and Figure 13 below respectively.

Table 5: values used for factors in second prototype head

Factor Code	Description	Second Prototype Value (in)
A	Duct-to-Bin Opening Width	7.7
B	Duct-to-Bin Opening Height	1
C	Duct-to-Bin Opening Fillet	0.2
D	Duct-to-Bin Opening Elevation (Location on Bin)	3
E	Head-to-Duct Opening Width	12.6
F	Head-to-Duct Opening Height	0.75

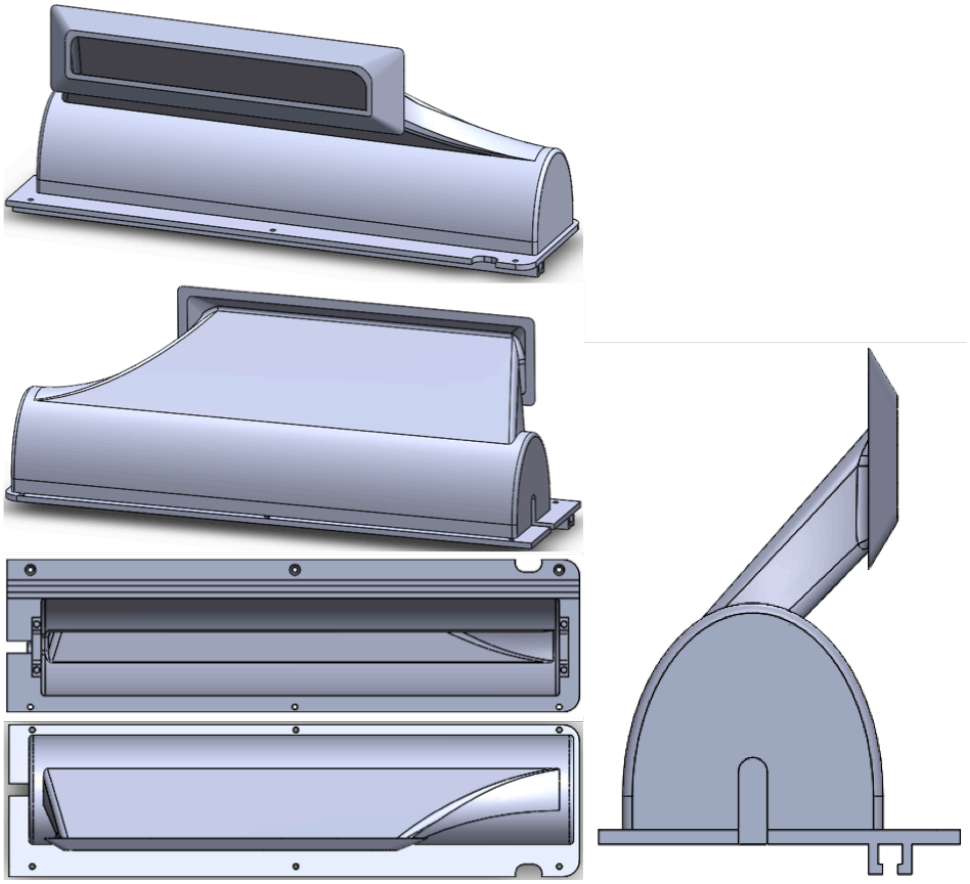

FIGURE 13: SECOND PROTOTYPE HEAD

The parameters for the second prototype head were arrived at by applying the same general lessons learned from the optimization of the first prototype's head parameters but also taking into account the new goal of extending the head to the wheel path and using the more flared duct shape. It is possible the parameters are therefore not completely optimized for this head geometry.

To increase the storage capacity of the bin, the elevation was increased such that incoming air would not be blowing around debris that had already settled to the bottom of the bin. Additionally, the bin was changed from one with a square cross-sectional area to a cylindrical bin with circular cross section for reasons that are explained in Benjamin Schilling's thesis. Since the connection between the bin and duct using a face seal with an o-ring was not very successful in the first prototype, this presented an opportunity for redesigning the seal for the rounded interface. Instead of having the face seal, the head

would be jammed into a second 3D printed part attached to the bin such that the difference between the tapering in the second part and that in the head's flange would create an appropriate seal.

Planning for the second prototype also included having space for the brush mounting to be somewhat adjustable by adding shims where the support parts of the brush screwed into the head. This setup is shown in Figure 14 below. In order to do this slots also had to be cut into the side of the heads that faced the middles such that the connector shaft could also be allowed to move up and down with the brush. Lastly, the back scraper that was made out of a rubber material in the first prototype was changed to a brush instead so that airflow would not be completely blocked and impedance would therefore be decreased. The mounting mechanism for this back scraper brush was also built into the head in the second prototype.

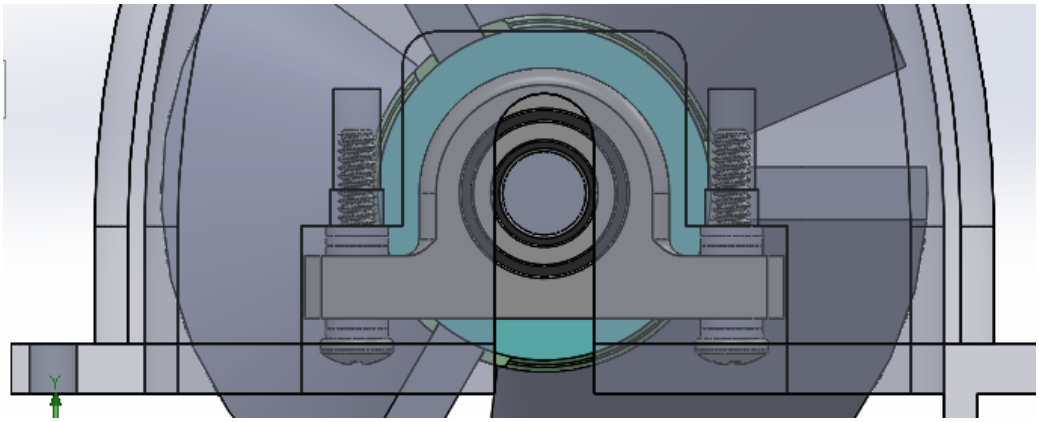

FIGURE 14: IMAGE OF BRUSH ADJUSTABILITY MECHANISM

Front Wall Extension

During very early testing of the first prototype, it was noticed that small objects such as screws were rejected by the vacuum and instead of being flung up into the head and duct, they were shot out the front of the robot by the brush's rotation. In an attempt to solve this problem, plans were made to add a small extension to the head's front wall so that some areas could have a smaller clearance between the floor and the head. The idea was to have some of these objects that were being flung out instead hit the wall extension and follow

the curve of the duct into the debris storage bin. Two designs of the front wall extension were created for the first prototype.

The first design was a 3D printed extension composed of a thin rectangle that ran all along the length of the front wall and on regular intervals there were rectangular extrusions coming off the rectangular piece and towards the floor. The purpose of the triangular pieces was to create a wedge that would push material towards the more open areas so that they could enter the space underneath the head and the flat backs of the rectangles would block part of the exit path and help the pieces move along the curve of the head. This design was briefly tested while the robot was stationary before it was decided that further thought would have to be put into the ratio of open space for objects to enter the head and closed space that would block exits from underneath the head. For this reason the second design iteration was created as a simpler front wall extension that did not require any initial optimization.

FIGURE 15: FIRST DESIGN ITERATION FOR THE FRONT WALL EXTENSION OF THE FIRST PROTOTYPE.

The second design iteration for the first prototype consisted 2 rectangles that were laser cut out of ¼" acrylic. The two rectangles were layered on top of each other and screw holes matching those that were already on the head were added and counterbored on the bottom rectangle. This created a flat wall of constant height that was then attached to the bottom of the head. The design is much simpler but has downsides in that the size of items that could pass under the wall was now very restricted. This second acrylic design was the main front wall extension used during testing of the first prototype.

For the second prototype, the first design with the 3D printed block holding the triangular pieces was brought back and the standard for the size of objects that should be able to fit through the front wall extension was set to be skittles. A large triangle spanning the area between the two heads was also added with slots for bristles so that objects that could

otherwise pass undisturbed in the area between the heads would instead be pushed towards one of the sides where the heads are located. Since skittles have a diameter of 0.43in, the spaces between triangles was set to 0.45in. The width of each triangle was set to about 0.75in. If the front wall extension did not have the wedges for moving objects into the open spaces the idea ratio of closed to open space would be 1:1 but due to the wedges, the new optimal ratio likely contains more closed space than open space. This is something that would need to be further optimized and the front wall extension was designed as a separate part even in the second prototype such that it could be switched out in the future for testing different ratios.

FIGURE 16: CAD OF FRONT WALL EXTENSION FOR SECOND PROTOTYPE.

Air Velocity Predictions

As previously mentioned, the CAD for the first prototype was updated as the build process progressed so as to maintain as accurate a CAD model as possible while adjustments were made during assembly. A final CFD simulation was run to obtain predictions of the air velocities that would be observed in the prototype. Figure 17 below shows the full velocity distribution that is expected according to the simulation. The main purpose of this final simulation was to compare the simulation results to those found through experimentation with the prototype. If the results were similar then the optimization via the CFD simulations, as opposed to building several head shapes and prototypes, is validated.

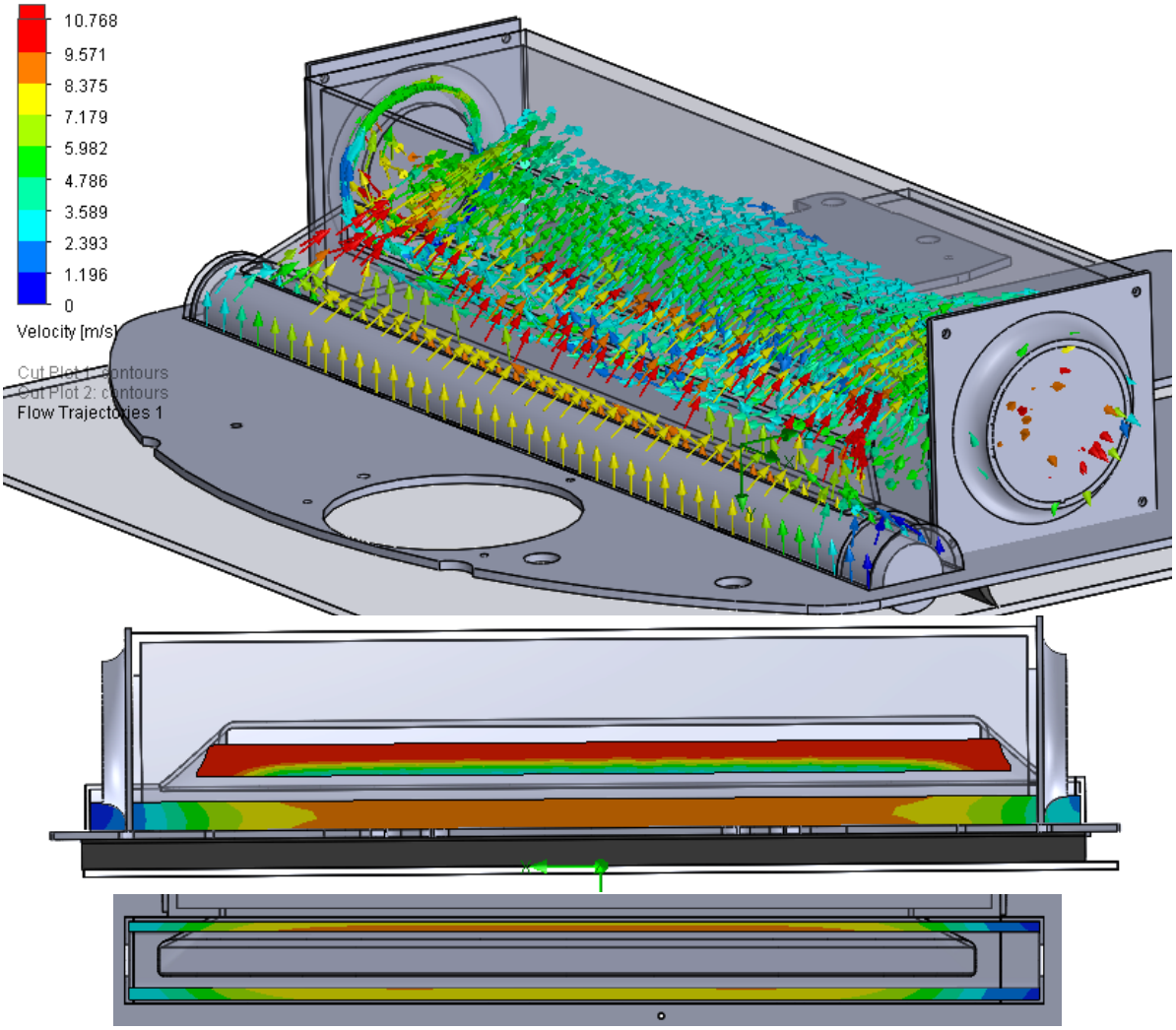

FIGURE 17: FINAL CFD SIMULATION WITH UPDATED PROTOTYPE DIMENSIONS, FAN MOUNTING PLATES, AND FILTER OUTLET SIZE CONSTRICTION. THE CUT PLOTS GIVE A BETTER VIEW OF THE VELOCITY DISTRIBUTION WITHIN THE DUCT AND AT THE ENTRANCE TO THE HEAD. THE SCALE IS THE SAME FOR ALL THE IMAGES SHOWN HERE.

As can be seen from Figure 17 above, even at the edges of the head it is expected that velocities of approximate 3m/s will be achieved. Notice that one edge that the head is asymmetric and one edge shows lower velocities but this corresponds to where the motor would be added and the actual vacuum section of the head does not extend that far in the prototype. These results are similar to those achieved through the final pre-prototyping CFD simulations, which also accounted for elements such as the shape of the fan mounts and the restricted filter outlet size. These final pre-prototyping CFD simulations were used

as a final check on making the decision to go ahead with the first prototype design since it appeared sufficient velocity could be achieved. Figure 18 below shows the expected velocity distribution at the head entrance and duct exit with the first prototype dimensions. The duct exit velocity predictions are the values that can be compared to the measurements taken on the prototype.

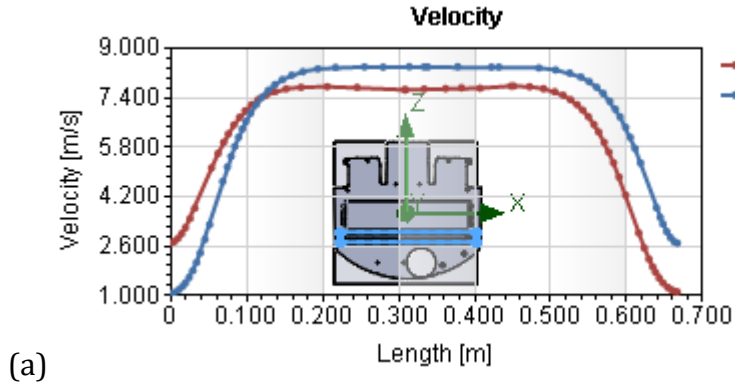

(a)

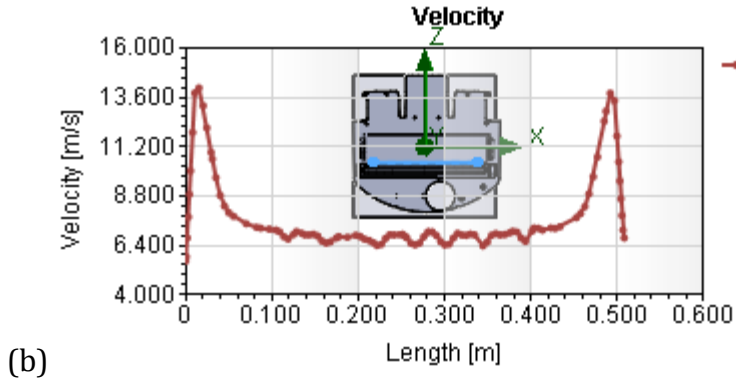

(b)

FIGURE 18: CFD SIMULATION VELOCITY PREDICTION AT THE (A) ENTRANCE TO THE HEAD AND (B) EXIT OF THE HEAD DUCT AND JOINT INTO THE BIN. THE BLUE LINES ON THE CAD MODELS SHOWN ON EACH GRAPH CORRESPOND TO THE LOCATIONS FOR WHICH THE VELOCITIES ARE PLOTTED. THE HEAD ENTRANCE HAS TWO LINES BECAUSE THE AIR CAN ENTER TO EITHER SIDE OF THE BRUSH AND BOTH LOCATIONS WERE PLOTTED.

When the fans are de-rated to 50% to serve as a simulation of dirty filters, the results show decreased velocities throughout. Figures 19 and 20 show the results in the overall CAD and the specific velocity distributions at the head entrance and duct exit. Notice that the velocity is still maintained at above 1m/s even at the edges on the head entrance. The general trends for the shape of the velocity distributions also remain as they were with the fan at its full capacity.

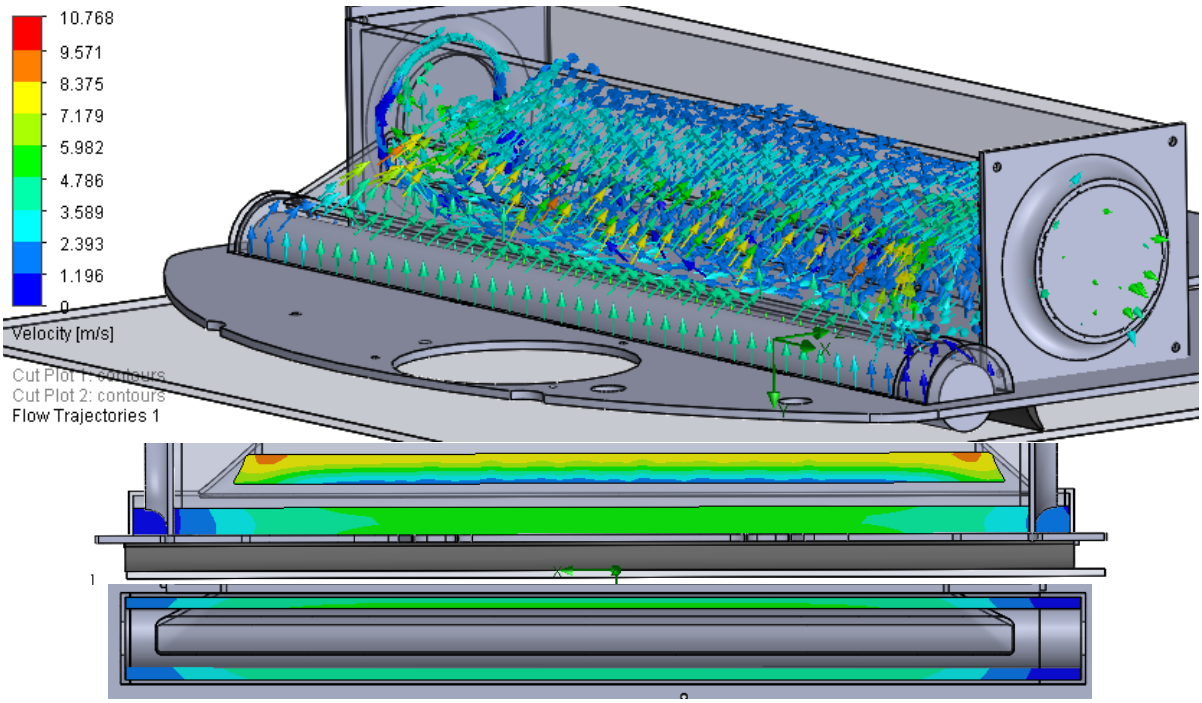

FIGURE 19: FINAL CFD SIMULATION WITH UPDATED PROTOTYPE DIMENSIONS, FAN MOUNTING PLATES, AND FILTER OUTLET SIZE CONSTRICTION PLUS DE-RATED FAN. THE CUT PLOTS GIVE A BETTER VIEW OF THE VELOCITY DISTRIBUTION WITHIN THE DUCT AND AT THE ENTRANCE TO THE HEAD. THE SCALE IS THE SAME FOR ALL THE IMAGES SHOWN HERE.

Although the velocity distribution looks more evenly distributed in the de-rated simulation, this is due only to the scaling used for the figure. The same scaling has been maintained the same as in Figure 17 to allow for better comparison. Since the velocities are overall lower in the de-rated simulation, the differences across the head entrance are also smaller and show up less in these images. Looking at the cross section of the duct, it is possible to see the beginning of the vena contracta forming at this point in the duct. This is likely what causes the sharp increase in velocity seen at the ends of the duct in Figure 20 below. Another reason for the sharp increase in velocity here is that the duct is wide at its connection with the head and becomes narrower towards the bin. This causes the airflow from the edges of the head and the edges of the duct at the connection to the head to compress into a smaller cross-sectional area as the air moves towards the bin. In fact, the cross sectional area of the duct has been designed to be as constant as possible throughout the duct but the need for non-symmetric streamlines across the plane perpendicular to the

air's movement causes this effect of higher velocity on the edges as the bin is approached anyway.

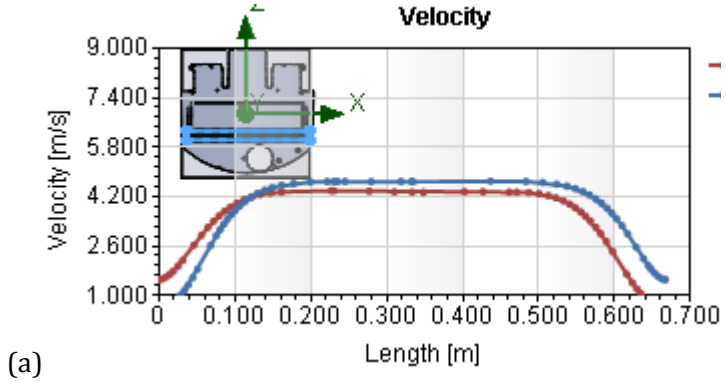

(a)

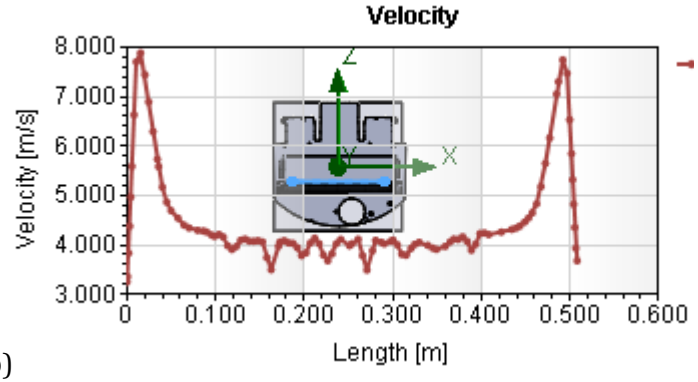

(b)

FIGURE 20: CFD SIMULATION WITH DE-RATED FANS - VELOCITY PREDICTION AT THE (A) ENTRANCE TO THE HEAD AND (B) EXIT OF THE HEAD DUCT AND JOINT INTO THE BIN. THE BLUE LINES ON THE CAD MODELS SHOWN ON EACH GRAPH CORRESPOND TO THE LOCATIONS FOR WHICH THE VELOCITIES ARE PLOTTED. THE HEAD ENTRANCE HAS TWO LINES BECAUSE THE AIR CAN ENTER TO EITHER SIDE OF THE BRUSH AND BOTH LOCATIONS WERE PLOTTED.

Prototyping & Building

Many of the parts used for the CFD Simulations and study could easily be transformed into manufacturable parts for the prototype with few if any changes. The brush was one of the main exceptions as it was modeled as a simple cylinder in the CFD studies

Brush

First Prototype

For the actual prototype there were two iterations of the brush design because the first iteration failed and a second therefore had to be developed during the prototype build

phase. The first iteration was one that incorporated commercially available brushes and the second was one that was custom made for this project. In both iterations of the brushes they were mounted at a level such that they were coaxial with the semicircular part of the head.

In the first iteration, it was decided that off-the shelf brushes would be used since part of the goal of the overall project was to make use of off-the-shelf parts where possible. Commercially available brushes that were also found to be appropriate for the robot design tended to be brushes that were sold as replacements for those in commercial vacuum cleaners. All of the options found were shorter the planned robot width and it was therefore decided that multiple Oreck vacuum brushes for the XL21 Series (12.375" wide) would be spliced together to create the project's brush. Since concentricity was a major concern, the design for splicing the brushes together used helical parts on the outside of the brushes to clamp together two at a time. The design is shown in Figure 21 below. By clamping from the outside less error would be introduced into the part than if the design instead relied on accurate centering of a dowel pin or shaft into the brush. This was especially a concern since it was not known whether the brushes were hollow or not during the initial planning step. The commercial brushes intended for existing vacuum cleaners also came with their own bearings, pulley, and belt so the need for purchasing these separately was eliminated. Parts for attaching the brush to the rest of the head by holding it from the bottom and screwing into the bottom of the head were designed such that the brush could be inserted from underneath the head. These parts as well as those for splicing the brushes together were 3D printed in PLA.

FIGURE 21: CAD OF THE FIRST BRUSH ITERATION

When the brushes were purchased and spliced together, testing revealed that the mechanism was not sufficiently stable to hold the brush while it spun. Part of the problem was caused by last minute changes that required one of the clamping mechanisms to join 3 instead of 2 sections of the commercial brush – one very short section and two longer ones. The wobbling of the brush joints cause interference with parts of the vacuum head and the shaft also interfered with the floor while rotating. This unstable system would quickly degrade itself over time and also caused a significant amount of noise generation so it was decided that a better brush design was necessary.

Since the joints between brushes appeared to be the main failure of the first brush design, this feature was eliminated in the second design which therefore could not be a commercially available brush. For this design a wooden shaft was therefore used as the main part of the brush. The wooden shaft was turned down slightly to achieve the desired diameter and better concentricity. Slots were cut to allow for bristles to be slid in to complete the brush design and bearings and a metal shaft were used to support the brush in the head frame. The same pulley and belt from the commercial brush were added to the end of the second iteration as these parts functioned sufficiently well in the test. The support parts used in the first iteration were adapted to hold bearings that the new brush's shafts could now pass through and the brush was again inserted from the bottom of the head. The design of the second iteration is shown in Figure 22 below. When installed this brush was much quieter and did not create interference problems.

FIGURE 22: CAD OF THE SECOND BRUSH ITERATION WITH THE SUPPORT PARTS AND SHAFTS

Second Prototype

The straight brush used in the first prototype proved to be quite efficient but many vacuum cleaners also use helical brushes to move debris towards a desired direction nearer to the

duct's connection to the head. In the case of this project a helical brush was also theorized to help the efficiency of the front wall extension design with triangular extrusions. This is because if a straight brush is used, it is likely that the objects entering the head space will be pushed out in a straight line and therefore will exit through the same space they entered. By using a helical brush, however, it is more likely that the object's path back towards the front of the head would be different than the path through which it entered. This would improve the chances of objects hitting the back of the triangular extrusions and moving into the head's space. For this reason, two types of brushes were designed for the second prototype, one straight and one helical. Both brushes were to be 3D printed and had T-slots for holding brush strips that were commercially available on McMaster Carr. Figure 23 below shows the two brush designs. Since the two heads of the second prototype were asymmetric and were mirrored versions of each other, the helical brushes were also printed as a mirrored pair such that one had a right handed helix and the other a left handed helix. This allowed for installation in such a manner that the brushes would push debris towards the center of the robot, where the ducts connected.

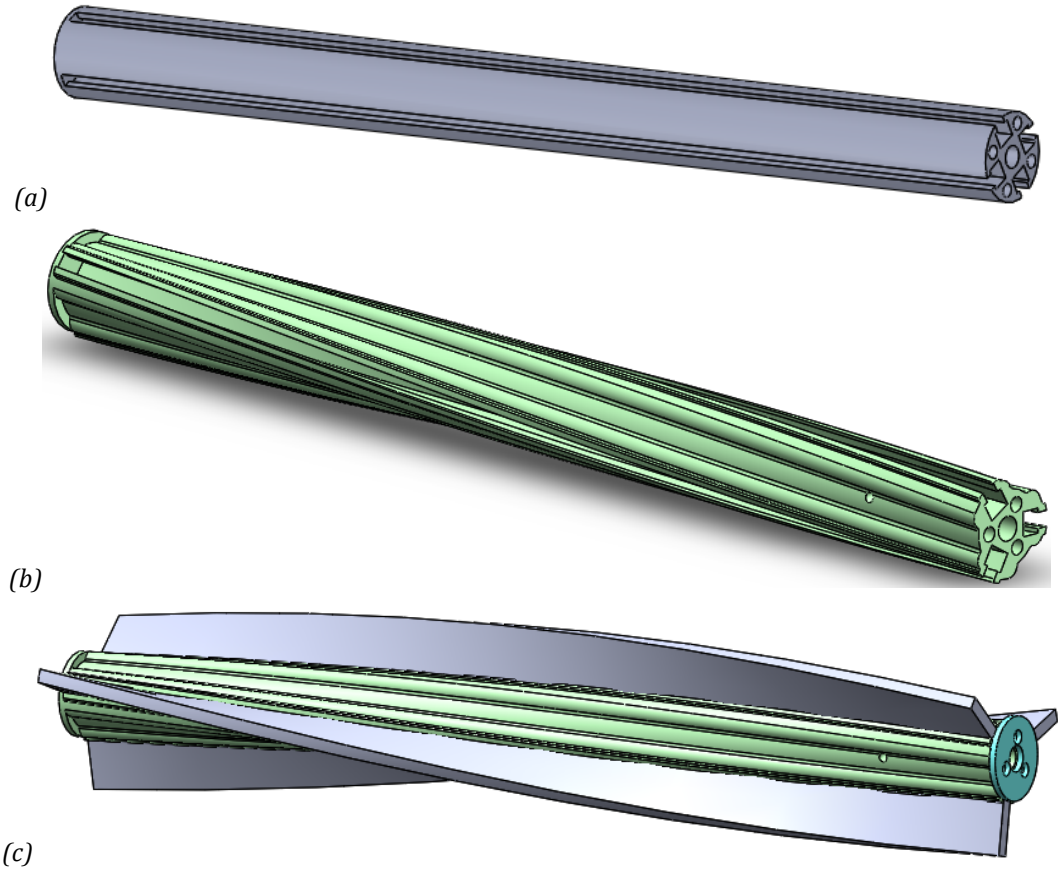

(a)

(b)

(c)

FIGURE 23: (A) STRAIGHT AND (B) HELICAL BRUSHES DESIGNED FOR THE SECOND PROTOTYPE. (C) SHOWS THE ASSEMBLY OF THE HELICAL BRUSH WITH THE BRISTLES MODELED IN AS A SOLID GREY STRIP. THE HELICAL BRUSH CONTAINS 3 SLOTS FOR THE BRISTLES AND THE STRAIGHT BRUSH HAS 4. BRUSH CAPS WERE INCLUDED IN THE DESIGN SO AS TO PREVENT THE BRISTLE STRIPS FROM SLIPPING OUT. ON ONE SIDE THE BRUSH CAP WAS BUILT INTO THE MAIN SHAFT SECTION AND ON THE OTHER SIDE THE BRUSH CAP WAS PRINTED SEPARATELY AND SCREWED ON AFTER THE BRISTLES ARE SLID IN.

Another benefit of the helical brush is that with this design some bristles would always be in contact with the floor. This decreases the instability of the brush as the constant force means an equilibrium in the position of the brush is more likely to be reached than with the forces that are applied to the straight brush each time a new set of bristles hits the floor. A constant force on the bristles also means that the motor is encountering a constant resistance upon rotating the brush so the speed of rotation will also likely be smoother with a helical brush than with a straight brush. To counteract the inconsistency of the forces on the straight brush, it was designed with as many slots for bristles as possible so

that there is as little time between each set of bristles touching down as possible. This creates a smoother rotation than using only two sets of bristles.

Head

For both the first and second prototypes, the heads were 3D printed out of ABS and were rubbed down with acetone so as to merge the layers and create a more airtight surface. Flanges were added at the bottom of the head with screw holes for securing the head to the main chassis plate.

For the first prototype the width of the head was too large for the printers at hand so the part was split into two with an overlapping section in the middle and the two halves were joined during assembly. A flange was also added so as to create a face seal against the bin side with an O-ring. Screw holes were also added to the top part of the flange but these were never used. The bottom part of the flange is not readily accessible for adding screws into.

Prototype Measurements & Testing

Performance tests were carried out to measure both the percent of pickup the vacuum robot could achieve and the linear velocity of air at the exit of the duct. Although a more complex design of the head front wall extension was tested on the robot while it was stationary, the simpler, acrylic design was used for the prototype measurements and testing.

Percent Pickup

The pickup performance tests were carried out according to the methodology previously outlined. The full data collected from the tests is shown in Appendix C. The main set of tests was carried out while the filters were already dirty and with the maximum fan speed setting (100%) and an 80% brush setting. Using dirty filters is reasonable as the filters very quickly get saturated with dust/dirt so most of the real operation time of such a robot would be with the filters in a relatively dirty/clogged state. A single pass over the area of interest was carried out in this main set of experiments and it therefore allowed for calculation of first-pass pickup. Additional tests were also carried out for 2-pass pickup and

for different brush settings. Lastly, some testing was also carried out on larger objects – washers and screws.

First-Pass Pickup

Eight experiments were carried out for determining the first-pass pickup at the settings mentioned for the main block of experiments: 100% fan speed, 80% brush speed, and flour as the debris simulator. The data from the eight experiments appeared to have at least one outlier so the generalized extreme Studentized deviate (ESD) test for outliers was carried out for k = 3 (as a conservative test)[15]. It was found that indeed the highest value in the range was an outlier but the other two values that were tested were not. Figure 24 below shows that by removing the outlier the data also looks to be relatively normally distributed. The data set was therefore adjusted to remove the outlier so that 7 tests remained for statistical analysis. The first pass pickup was therefore found to be approximately 63% with a standard deviation of 6%, yielding a 1σ range of 57% to 69%.

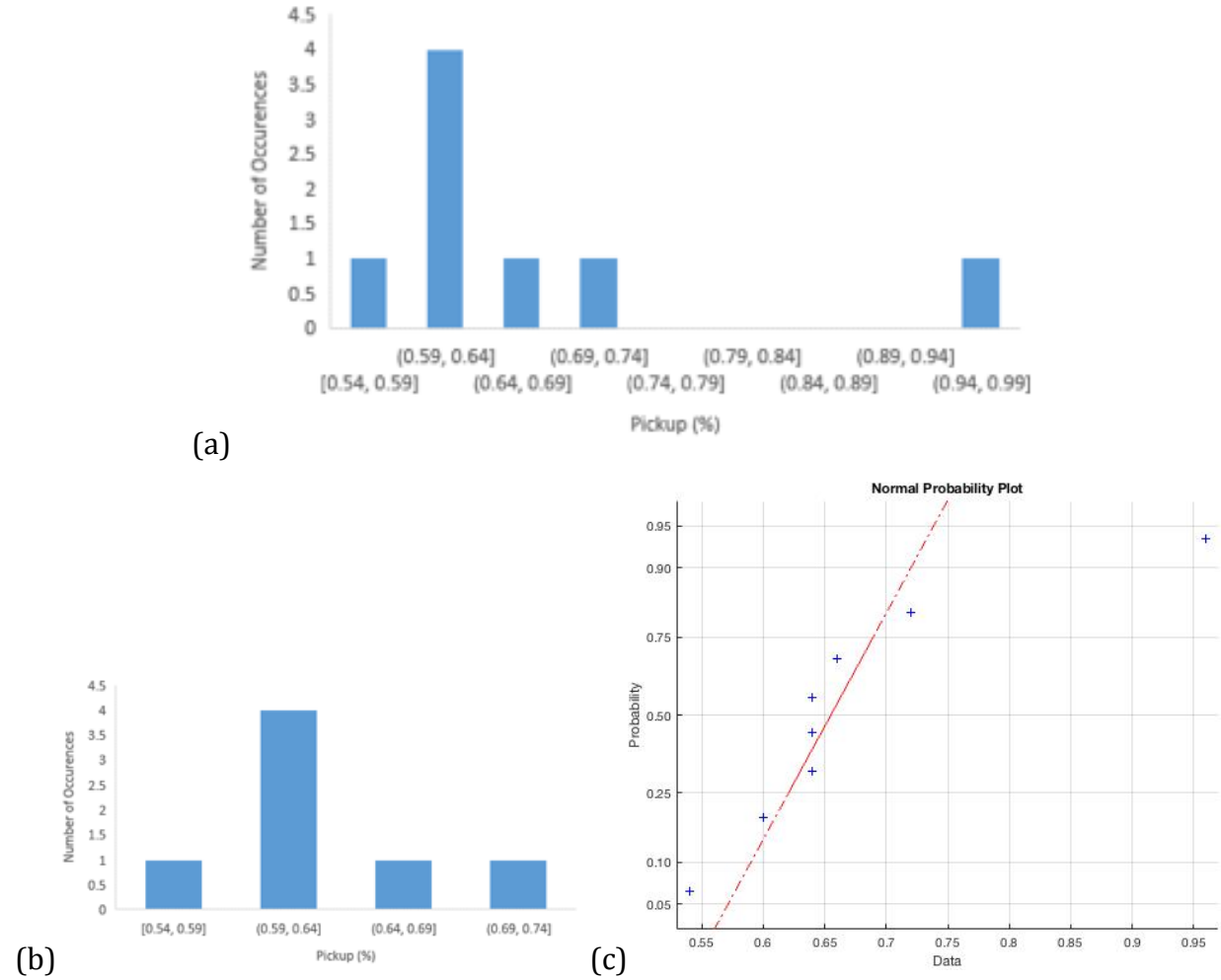

FIGURE 24: HISTOGRAMS SHOWING DATA DISTRIBUTION FROM THE MAIN SET OF EXPERIMENTS. (A) SHOWS THE HISTOGRAM WITH THE FULL DATA AND (B) SHOWS THE HISTOGRAM WITH THE OUTLIER REMOVED. (C) IS THE NORMAL PROBABILITY PLOT WHERE THE FULL SET OF DATA IS PLOTTED, INCLUDING THE OUTLIER, WHICH APPEARS AS THE RIGHT-MOST POINT. THE DATA LOOKS TO BE AT LEAST SOMEWHAT NORMAL, BUT MAY HAVE A SLIGHT SKEW TO THE RIGHT.

One experiment was carried out with the brush setting decreased to 47% while all other variables were maintained constant and the first-pass pickup rate obtained was 28%. Increasing the brush setting to 100%, on the other hand, also increased the first-pass pickup to 86% in one experiment. Assuming a normal distribution and constant variance for the set of 7 data from the moderate brush speed experiments, there is about a 0.1% chance and a 7% chance of the additional experiments at different brush speeds yielding these pick-up values randomly. It is therefore very probably that the brush speed indeed

has an impact on the pick-up rate and the preliminary data indicates that an increase in brush speed increases pick-up. It is not clear whether the change from 80% brush speed to 100% brush speed had a significant impact as it does not have a significance level of 5% or below but it does meet the requirement for significance of 10% or below. The results of the first pass experiments are summarized in Table 6 below.

Table 6: Summary of first-pass experiments

# Of Samples	Brush Setting (%)	Average Pick-Up (%)	Standard Deviation (%)
1	47	28	-
7	80	63	6
1	100	86	-

If a quadratic model is fit to the data to find the relationship between brush speed and debris pick-up, the result is Equation 4 below. The fit is plotted below along with the average values and the raw data.

Equation 4: vacuum debris pickup vs. brush speed where x is the brush setting in percent.

$$Pickup = -15.5066 + 0.8464x + 0.0017x^2$$

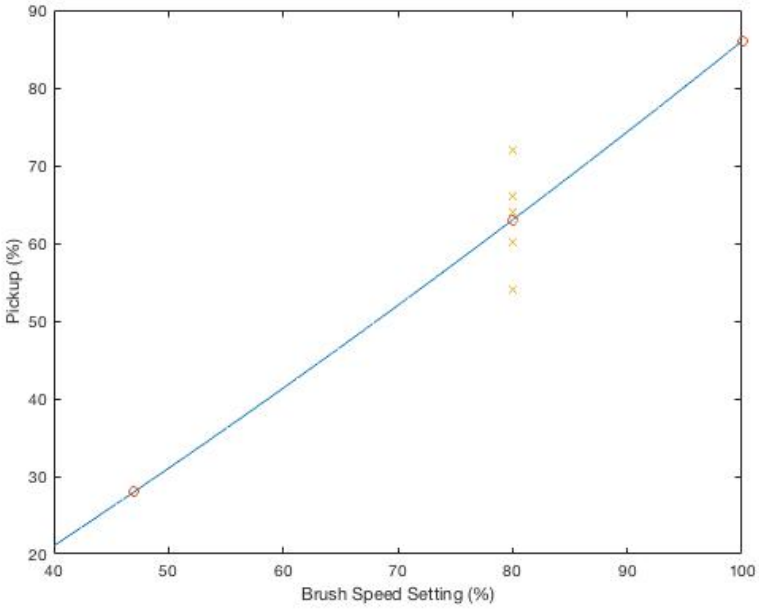

FIGURE 25: QUADRATIC FIT OF THE BRUSH SETTING VS. PICKUP. THE CIRCLES SHOW THE AVERAGE VALUES LISTED IN TABLE 6 ABOVE AND THE X'S SHOW THE RAW DATA FOR THE EXPERIMENTS AT 80% BRUSH SPEED.

Interestingly, it appears that the effect of the brush speed may actually be one of the most important variables in the head design as one experiment that was run using only the brush at 100% speed and no fans was still able to achieve 32% pickup. Only one experiment was run under these conditions so more data would have to be collected to confirm the strong effect of the brush. The pickup rate during this experiment is also interesting because it was higher than the experiment that was run with the fans turned on and the brush at 47% speed. This would suggest that there might be some conflicting interaction between the fans and brush rotation.

Second-Pass Pickup

A set of three experiments was carried out to test second pass pickup. All the experiments were again carried out with the brush speed set at 80% and the fans set at 100%, flour as the debris simulator, a dirty filter, and the simple acrylic design for the head front wall extension. The full data for the second pass tests are shown in Appendix C. The average pickup achieved was 84% with a standard deviation of 5%. Under these conditions, the hypothesis that the second-pass pickup is equivalent to the first-pass pickup cannot be rejected since if the robot were to pick up 63% on the first pass and 63% of the remainder on the second pass, an overall 2-pass pickup of 86% would be expected.

Picking up Objects

To test the ability of the vacuum to pickup objects in addition to fine debris like flour and dust, a couple of tests were run without flour and using washers and screws instead. The first test used the same settings as the main set of experiments: 80% brush speed setting, 100% fan speed setting, the simply acrylic design for the head front extension, and dirty filters. In the first test 20 a4 2.5mm washers were spread over the robot's path and it was able to pick up 2 washers (10% pickup rate) with one pass. Due to low clearance between the acrylic front head extension and the floor screws were not able to fit under to reach the head entrance and it appeared as though many of the washers also didn't fit through as they were all lined up under the robot at the end of the test. This means the washers were probably pushed by the head front wall extension and did not go under. 2 of the washers

were flung out from underneath the robot by the brush but 16 of the 20 were found lined up in this way at the end of the test.

In a second attempt to test the vacuum's ability to pick up objects an extra test was run with a modification made to the head front wall extension. The extension was shortened by removing the first layer of acrylic and using only the counterbored layer. The test was run again with 10 a4 2.5mm washers and 10 screws. The robot was able to pick up 1 washer and 2 screws in this test and did not seem to push any of the material with the wall extension. However, the test was not fully successful as the brush stopped working part of the way through. Due to time constraints, no more tests were carried out.

Velocity Measurements

Figure 26 below shows the results of the velocity measurements carried out at each of the approximate locations on the duct exit. It was found that with the brush motor turned off there was significant variation in the velocity that was measured depending on the position of the brush. During measurements an attempt was made to capture the maximum velocity that could be achieved with the brush motor turned off. When the brush motor was turned on some fluctuation was still seen but measurements were significantly more stable than with the brush stationary at different positions. The full set of data collected for the velocity measurements is shown in Appendix D and it shows some of the fluctuations that have been discussed here.

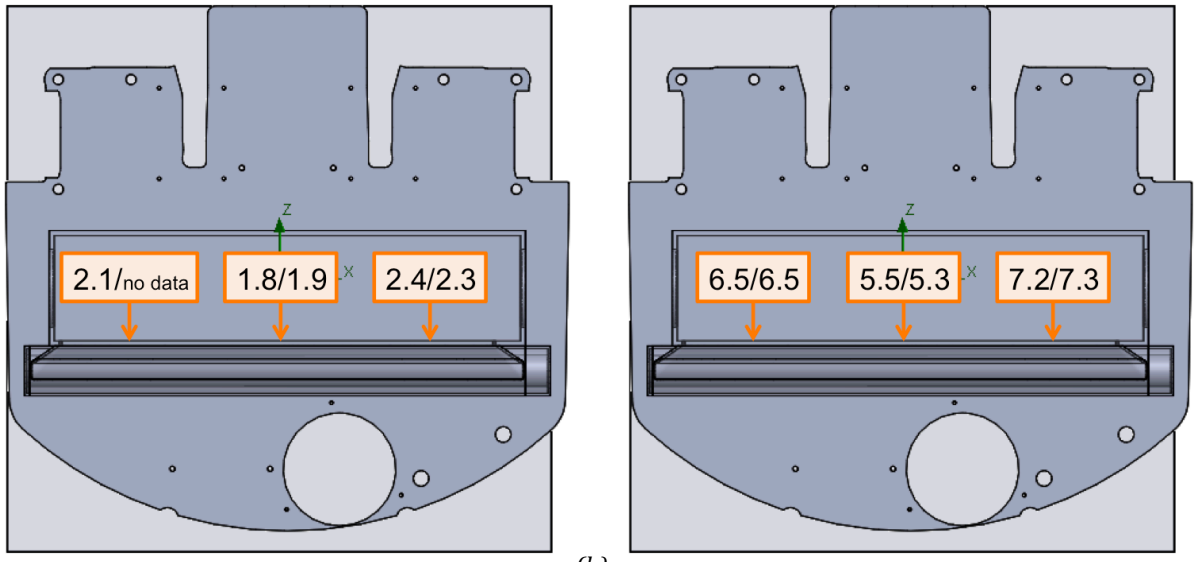

(a) *(b)*

FIGURE 26: VELOCITY MEASUREMENTS TAKEN WITH (A) DIRTY FILTERS AND (B) CLEAN FILTERS. THE FIRST MEASUREMENT SHOWN WAS TAKEN WHILE THE BRUSH MOTOR WAS TURNED ON TO 80% POWER AND THE SECOND MEASUREMENT WAS THE MAXIMUM ACHIEVED WITH THE BRUSH MOTOR TURNED OFF. ALL UNITS ARE IN M/S.

Since one of the pickup tests had showed that debris could be picked up even when the fans were turned off, a velocity measurement was also taken with the fans turned off and the brush roller setting at 80%. The filters were clean for this experiment but this should not have a large impact on the result and if it did, it would decrease impedance and therefore yield a higher flow rate. However, the measurement taken at the right side of the duct exit with the fans turned off yielded a velocity of zero. No other measurements were taken at the other points of the duct exit.

Chapter 5: Results & Discussion

Comparison of Simulation Predictions and Test Results

Results obtained during the velocity measurements of the first prototype with clean filters are within 20% of the velocities predicted using the CFD simulation for the center of the duct exit and it appears that both also show similar trends of increasing velocity towards the outsides of the duct. This agreement between the simulation and the measured values somewhat validates the use of simulation for optimization of the head shape as an accurate one.

Additionally it can also be seen that when the filters become dirty the velocity at the duct exit appears to drop to 1/3 the velocities achievable with clean filters. This would suggest that de-rating the fans should indeed be a useful method to simulate a dirty filter while maintaining calculation times low. During the first prototype simulations, however, it was assumed that by de-rating the fan to 50% of its capability an accurate simulation of the prototype with dirty filters could be carried out. The data suggests that in fact, dirty filters can be simulated by de-rating the fan such that it retains only 33% of its original capability.

Brush Contributions to Airflow and Debris Pickup

The contribution of brush to airflow was not very clear in the velocity measurements taken at the exit duct. In some sets of measurements the velocity with the brush turned on was higher and in others the velocity was higher with the brush turned off. Due to the variation seen during the measuring process, it is not possible to say whether these small differences are real or not. Interestingly, however, the brush did appear to be very useful in picking up debris in one experiment even when not paired with the fans. Further studies are needed before any decisive conclusions can be drawn from the one experiment carried out in this study.

For now it would seem that continuing to carry out the CFD simulation studies without simulating the brush and its rotation can still provide sufficiently accurate predictions of air flow. Additionally, the fact that, when stationary, the brush can have a visible effect on the velocity of air exiting the duct points at another potential benefit of having helical

brushes. When straight brushes rotate within the head there are instants when the brush will be located in an unfavorable position for airflow by decreasing the clearance between the brush and the inside of the head. If this is the case a helical brush could also be preferable because although there will always be bristles that create a small clearance with the inside of the head, there could also always be a path that leads to the duct such that the air does not have to travel through the low clearance area. This effect is not known to exist and it is possible that the reverse could also be true and that airflow rate and brush shape are also related by the third factor of brush rotational speed.

Front Wall Extension Performance

The front wall extension definitely improved the retention rate for small objects like washers and screws, which were not picked up at all by the vacuum robot prior to the installation of the extension. The uneven warehouse floors, however, are a relatively large issue when considering the front wall extension because the purpose is to have a very small clearance with the floor at the sections that are made for keeping objects from being flung outward. It is difficult to maintain this small clearance without having interference occur when the robot travels over uneven patches.

Although the 3D printed extension was not tested on the moving robot, it achieved good performance on stationary tests and was therefore recommended as the base design for the second prototype extension. The simple acrylic extension is also expected to perform worse than the 3D printed design with the triangular extrusions because it only allows in objects that also have a high chance of making it out without being captured by the extension and moved up into the head and duct area. Even with the lower performance acrylic extension, however, some pickup of small washers and screws was achieved, which is a good sign indicating that with some extra work this solution could have a high benefit for the robot.

Effect of Multiple Passes

From the data obtained from 1-pass and 2-pass experiments it would appear that each pass is for the most part independent of previous passes. This can be seen from the fact that the

2-pass experiments yielded a pickup rate that was approximately equivalent to having the 1-pass pickup rate during each pass. This is good news because it means that performance is maintained on subsequent passes and that the vacuum robot is not making the task of further cleaning more difficult for the areas where it passes. Ideally the robot would be able to increase its pickup rate on a second pass because the first pass loosened some dust that was still left behind and can be picked up more easily on the second round. It is still possible that this may be the case but because tests were carried out with flour that was dropped on the floor immediately prior to testing, the debris being tested was not necessarily as stuck to the floor as it may be in some warehouses that have not received cleaning for some months. Hopefully, however, with a cleaning robot such as the one developed in this project, warehouse floors would not progress to the point where the debris strongly adheres to the floors.

Chapter 6: Conclusion & Future Work

The resulting product of this project is a vacuum cleaner robot with a nearly optimized head and duct shape and the capability to perform on the same level as many commercially available vacuums while also being adaptable to a warehouse, industrial environment. The work done in this project has already yielded a product that can be distinguished from other cleaning robots on the market due to its ability to fit in smaller spaces and under some overhangs as well as its quick cleaning speed. Additional studies are recommended for certain aspects of the project, however, and these are discussed briefly below.

Suspended Cleaning Head

Due to irregularities in most industrial floors, including the floor that testing was carried out on for this project, it was difficult to calibrate the location of the head and brush in such a way that it fit the cleaning needs of the entire floor. For this reason, it is recommended that for future developments of this or similar projects, the head should be placed on a suspension system. Ideally this suspension system would allow for the whole head to move up and down within a range equivalent to or greater than the range of fluctuation in the floor level. Additionally, this movement should be allowed even in scenarios where the two ends of the heads and brushes would not be on the same level. A system that simply contained springs on each side and a slot for the head and brush assembly to move in would likely not be enough as it would not allow for this full flexibility in movement and would likely lead to jams as the robot traversed areas where the right and left sides of the floor are at different levels. It is suggested that a four-bar linkage be considered as a possible solution for creating this flexibility.

Front Wall Extension Optimization

As previously mentioned, the balance between the space left open and that which is closed off in the front wall extension likely has a large impact on what kind of small objects are picked up by the robot and the percent pickup rate for these objects. It is therefore suggested that more experiments be carried out using different ratios of open to closed space and also exploring different base designs than the one currently used. For such a study it would be ideal to pick one or a few target small objects to study and for which to

optimize the system. The small objects of highest importance would likely vary from warehouse to warehouse so this study would likely be more personalized to a specific location.

Brush Studies

The second prototype of this project was planned to include a set of helical and a set of straight brushes but these were not tested independently. It is suggested that studies be carried out to see the effects of each brush on airflow as well as on the ability to pick up different types of debris and small objects. Additional studies into the relationship between brush rotation speed and airflow rate or air velocity might also be interested as the current data appears to show a quadratic relationship, which could yield interesting results at more extreme brush speeds than the ones which were tested here.

Picking up liquids

Amongst, the loose products that sometimes finds its way to the floors of warehouses there will be some that are containers for liquid materials that break or open when falling out of the pods and spill the contents. Liquids are probably amongst the most harmful type of loose product as it can be accidentally spread by other robots and even if the floor is shut down for cleanup before spreading occurs, it is still more difficult to pickup/cleanup than most solid products. It would therefore be useful to develop a mechanism that could pick up liquid spills in addition solid debris. The same vacuum mechanism could be adapted to be amphibious or an independent mechanism could be developed for liquid spills.

If an independent mechanism is created, it could possibly be mounted on the same robot as the vacuum if space allowed for such a setup. In this case, the mechanism would be placed ahead of the current vacuum setup so that liquid spills could be cleaned up before the vacuum reaches them. This is important because if liquid spills come in contact with the vacuum mechanism and brush, it is likely that there will be significant spreading of the spill, even more so than with a regular warehouse robot. Additionally, the vacuum mechanism is not made to deal with liquid spills and if liquid reaches the filters it could be potentially damaging. Since first pass pickup of the liquid spills probably would not be

guaranteed by this system it would therefore also be necessary to be able to turn the vacuum mechanism on and off and lift it off the ground while it is off so that spreading does not occur. Additionally, since the wet cleaning mechanism would need to be placed ahead of the current vacuum setup, space reassignment would have to be carried out as space is made for this mechanism and other components of the drive and vacuum are relocated.

This page intentionally left blank

REFERENCES

[1] “DuoBot 1850 Specifications Sheet.” TASKI Intellibot. [Online]. Available: https://www.intellibotrobotics.com/downloads/DuoBot_Specs.pdf. [Accessed: 22-Jul-2017]

[2] “SwingoBot 1650 Specifications Sheet.” TASKI Intellibot. [Online]. Available: https://www.intellibotrobotics.com/downloads/SwingoBot_Specs.pdf. [Accessed: 22-Jul-2017]

[3] “AeroBot 1850 Specifications Sheet.” TASKI Intellibot. [Online]. Available: https://www.intellibotrobotics.com/downloads/AeroBot_Specs.pdf. [Accessed: 22-Jul-2017]

[4] S., “New Makita Cordless RobotPro Vacuum – a Heavy Duty Roomba-Like Cleaner,” ToolGuyd, 16-Jun-2016. [Online]. Available: http://toolguyd.com/makita-robotpro-vacuum-robotic-cleaner/. [Accessed: 22-Jul-2017].

[5] “Makita RobotPRO Robot Vacuum is the Next-Gen Shopvac,” Robotics Trends, 17-Jun-2016. [Online]. Available: http://www.roboticstrends.com/article/makita_robotpro_robot_vacuum_is_the_next_gen_shopvac/cleaning. [Accessed: 22-Jul-2017].

[6] “Makita 18-Volt X2 LXT Lithium-Ion (36-Volt) Brushless Cordless Robotic Vacuum Kit (5.0Ah)-DRC200PT,” The Home Depot. [Online]. Available: http://www.homedepot.com/p/Makita-18-Volt-X2-LXT-Lithium-Ion-36-Volt-Brushless-Cordless-Robotic-Vacuum-Kit-5-0Ah-DRC200PT/301282151?cm_mmc=Shopping%7CTHD%7Cgoogle%7CD29%2BAppliances&mid=sCLZiw1Yi%7Cdc_mtid_8903tb925190_pcrid_175068454992_pkw__pmt__product_301282151_slid_&gclid=CjwKCAjwqIfLBRAkEiwAhtfH68XVz-iIGc1vUDT1YXdtOGFuCF6y6dFdVVHBTztr1c6Om3zkxsqyvxoCW0QQAvD_BwE. [Accessed: 22-Jul-2017].

[7] “Product Details -DRC200Z,” Makita USA. [Online]. Available: https://www.makitatools.com/products/details/DRC200Z. [Accessed: 22-Jul-2017].

[8] Osha.gov. (2017). OSHA Fact Sheet: Laboratory Safety Noise | Occupational Safety and Health Administration. [Online] Available at: https://www.osha.gov/Publications/laboratory/OSHAfactsheet-laboratory-safety-noise.html [Accessed 11 Jul. 2017].

[9] Schilling, B. (2017). Robotic Vacuum Cleaner Design to Mitigate Slip Errors in Warehouses.

[10] Sobachkin, D. and Dumnov, D. (2014). Numerical Basis of CAD-Embedded CFD. [online] pp.1-16. Available at: http://www.solidworks.com/sw/docs/Flow_Basis_of_CAD_Embedded_CFD_Whitepaper.pdf [Accessed 15 Jul. 2017].

[11] Saad, Y. (1996). Iterative methods for sparse linear systems, PWS Publishing Company, Boston.

[12] Hackbusch, W. (1985). Multi-grid Methods and Applications, Springer-Verlag, NY, USA.

[13] “Max. 390 DC centrifugal fans Ø 120 x ... - Mouser Electronics.” [Online]. Available: http://www.bing.com/cr?IG=32A93FAA9F0644A9B56D2E7EBAEEF0D9&CID=3D7F52926871611937B75842697760BE&rd=1&h=t1ppEdOMLGhoqI9EAGpLPwlDR6ILf3qu

YSVim5St1xY&v=1&r=http%3a%2f%2fwww.mouser.com%2fds%2f2%2f120%2fRER120TD-934165.pdf&p=DevEx,5040.1. [Accessed: 15-Jun-2017].
[14] *Perry's Chemical Engineers' Handbook,* 8th ed, McGraw-Hill Professional Publishing, 2007,New York, NY,pp.788-790
[15] *Engineering Statistics Handbook,* National Institute of Standards and Technology. Gaithersburg, MD, pp.282-285

Appendices

Appendix A – Steepest Ascent Optimization Steps

A	B	C	D	E	F	gA	gB	gC	gD	gE	gF	New A	New B	New C	New D	New E	New F	Predicted Velocity
20.00	0.75	0.15	4.25	23.00	1.80	887.24	31535.40	8584.85	-6247.75	429.46	14794.55	20.09	3.90	1.01	3.63	23.04	3.28	320744.10
20.09	2.00	0.50	3.63	23.04	2.20	897.95	89085.00	17565.93	-6099.55	418.84	20103.35	20.18	2.00	0.50	3.02	23.08	2.20	81893.54
20.18	2.00	0.50	3.02	23.08	2.20	906.71	89520.25	17222.40	-5273.32	419.04	20107.64	20.27	2.00	0.50	2.49	23.13	2.20	91230.54
20.27	2.00	0.50	2.49	23.13	2.20	914.46	89897.30	16923.18	-4559.13	419.74	20110.82	20.36	2.00	0.50	2.03	23.17	2.20	99014.47
20.36	2.00	0.50	2.03	23.17	2.20	921.33	90224.05	16662.26	-3941.80	420.87	20113.05	20.45	2.00	0.50	1.64	23.21	2.20	105532.65
20.45	2.00	0.50	1.64	23.21	2.20	927.45	90507.32	16434.45	-3408.18	422.37	20114.45	20.55	2.00	0.50	1.30	23.25	2.20	111014.08
20.55	2.00	0.50	1.30	23.25	2.20	932.92	90753.00	16235.23	-2946.93	424.20	20115.14	20.64	2.00	0.50	1.00	23.30	2.20	115642.21
20.64	2.00	0.50	1.00	23.30	2.20	937.83	90966.19	16060.75	-2548.23	426.30	20115.20	20.73	2.00	0.50	0.75	23.34	2.20	119564.81
20.73	2.00	0.50	0.75	23.34	2.20	942.26	91151.30	15907.63	-2203.60	428.64	20114.72	20.83	2.00	0.50	0.53	23.38	2.20	122901.52
20.83	2.00	0.50	0.53	23.38	2.20	946.28	91312.15	15772.97	-1905.71	431.19	20113.78	20.92	2.00	0.50	0.50	23.42	2.20	123403.16
20.92	2.00	0.50	0.50	23.42	2.20	947.95	91336.80	15742.19	-1869.81	434.81	20110.31	21.02	2.00	0.50	0.50	23.47	2.20	123512.07
21.02	2.00	0.50	0.50	23.47	2.20	949.31	91342.32	15725.98	-1870.73	438.59	20106.48	21.11	2.00	0.50	0.50	23.51	2.20	123621.57
21.11	2.00	0.50	0.50	23.51	2.20	950.68	91347.86	15709.74	-1871.64	442.36	20102.64	21.21	2.00	0.50	0.50	23.56	2.20	123731.67
21.21	2.00	0.50	0.50	23.56	2.20	952.08	91353.40	15693.46	-1872.56	446.12	20098.78	21.30	2.00	0.50	0.50	23.60	2.20	123842.37
21.30	2.00	0.50	0.50	23.60	2.20	953.49	91358.95	15677.15	-1873.48	449.89	20094.92	21.40	2.00	0.50	0.50	23.65	2.20	123953.67
21.40	2.00	0.50	0.50	23.65	2.20	954.92	91364.51	15660.81	-1874.39	453.65	20091.04	21.49	2.00	0.50	0.50	23.69	2.20	124065.60
21.49	2.00	0.50	0.50	23.69	2.20	956.37	91370.09	15644.44	-1875.31	457.41	20087.16	21.59	2.00	0.50	0.50	23.74	2.20	124178.14
21.59	2.00	0.50	0.50	23.74	2.20	957.83	91375.67	15628.03	-1876.22	461.17	20083.26	21.68	2.00	0.50	0.50	23.78	2.20	124291.31
21.68	2.00	0.50	0.50	23.78	2.20	959.32	91381.26	15611.59	-1877.14	464.92	20079.36	21.78	2.00	0.50	0.50	23.83	2.20	124405.11
21.78	2.00	0.50	0.50	23.83	2.20	960.82	91386.86	15595.11	-1878.05	468.67	20075.44	21.88	2.00	0.50	0.50	23.88	2.20	124519.55
21.88	2.00	0.50	0.50	23.88	2.20	962.34	91392.47	15578.60	-1878.97	472.42	20071.51	21.97	2.00	0.50	0.50	23.92	2.20	124634.64
21.97	2.00	0.50	0.50	23.92	2.20	963.88	91398.09	15562.05	-1879.88	476.17	20067.58	22.00	2.00	0.50	0.50	23.97	2.20	124684.39
22.00	2.00	0.50	0.50	23.97	2.20	966.09	91399.87	15556.25	-1879.96	476.36	20065.93	22.00	2.00	0.50	0.50	24.02	2.20	124707.05
22.00	2.00	0.50	0.50	24.02	2.20	968.56	91400.08	15554.87	-1879.70	475.09	20065.23	22.00	2.00	0.50	0.50	24.07	2.20	124729.59
22.00	2.00	0.50	0.50	24.07	2.20	971.03	91400.28	15553.49	-1879.44	473.83	20064.53	22.00	2.00	0.50	0.50	24.11	2.20	124752.01
22.00	2.00	0.50	0.50	24.11	2.20	973.50	91400.49	15552.12	-1879.18	472.57	20063.84	22.00	2.00	0.50	0.50	24.16	2.20	124774.31
22.00	2.00	0.50	0.50	24.16	2.20	975.95	91400.69	15550.75	-1878.92	471.31	20063.14	22.00	2.00	0.50	0.50	24.21	2.20	124796.50
22.00	2.00	0.50	0.50	24.21	2.20	978.41	91400.89	15549.38	-1878.66	470.06	20062.45	22.00	2.00	0.50	0.50	24.25	2.20	124818.56
22.00	2.00	0.50	0.50	24.25	2.20	980.85	91401.09	15548.02	-1878.40	468.81	20061.76	22.00	2.00	0.50	0.50	24.30	2.20	124840.51
22.00	2.00	0.50	0.50	24.30	2.20	983.29	91401.30	15546.66	-1878.14	467.56	20061.07	22.00	2.00	0.50	0.50	24.35	2.20	124862.34
22.00	2.00	0.50	0.50	24.35	2.20	985.72	91401.50	15545.30	-1877.88	466.32	20060.38	22.00	2.00	0.50	0.50	24.39	2.20	124884.06
22.00	2.00	0.50	0.50	24.39	2.20	988.14	91401.70	15543.95	-1877.63	465.08	20059.70	22.00	2.00	0.50	0.50	24.44	2.20	124905.66
22.00	2.00	0.50	0.50	24.44	2.20	990.56	91401.90	15542.60	-1877.37	463.84	20059.01	22.00	2.00	0.50	0.50	24.49	2.20	124927.15
22.00	2.00	0.50	0.50	24.49	2.20	992.97	91402.10	15541.25	-1877.12	462.61	20058.33	22.00	2.00	0.50	0.50	24.53	2.20	124948.52
22.00	2.00	0.50	0.50	24.53	2.20	995.38	91402.30	15539.91	-1876.86	461.37	20057.65	22.00	2.00	0.50	0.50	24.58	2.20	124969.78

22.00	2.00	0.50	0.50	24.58	2.20	997.78	91402.49	15538.58	-1876.61	460.15	20056.97	22.00	2.00	0.50	0.50	24.63	2.20	124990.92
22.00	2.00	0.50	0.50	24.63	2.20	1000.17	91402.69	15537.24	-1876.36	458.92	20056.30	22.00	2.00	0.50	0.50	24.67	2.20	125011.96
22.00	2.00	0.50	0.50	24.67	2.20	1002.56	91402.89	15535.91	-1876.10	457.70	20055.62	22.00	2.00	0.50	0.50	24.72	2.20	125032.88
22.00	2.00	0.50	0.50	24.72	2.20	1004.94	91403.09	15534.58	-1875.85	456.49	20054.95	22.00	2.00	0.50	0.50	24.75	2.20	125047.54
22.00	2.00	0.50	0.50	24.75	2.20	1006.61	91403.23	15533.65	-1875.68	455.63	20054.48	**22.00**	**2.00**	**0.50**	**0.50**	**24.75**	**2.20**	**125047.54**

Appendix B - CFD Simulation Results for the First Prototype

A	B	C	D	E	F	Simulation Result (Velocity in m/s)
0.5588	0.0508	0.0127	0.0127	0.5715	0.03302	6.06E-09
0.0508	0.01905	0.00127	0.10795	0.0635	0.03302	0.000259857
0.5588	0.01905	0.00127	0.10795	0.5715	0.03302	1.09025743
0.0508	0.0508	0.00127	0.0762	0.0635	0.03302	0.000193793
0.5588	0.0508	0.00127	0.0762	0.5715	0.03302	1.30209355
0.0508	0.01905	0.009271	0.10795	0.0635	0.03302	0.000429125
0.5588	0.01905	0.009271	0.10795	0.5715	0.03302	3.85E-08
0.0508	0.0508	0.0127	0.0762	0.0635	0.03302	0.000139354
0.5588	0.0508	0.0127	0.0762	0.5715	0.03302	1.29337557
0.0508	0.01905	0.00127	0.10795	0.62865	0.03302	3.84E-09
0.5588	0.01905	0.00127	0.10795	0.62865	0.03302	2.34415737
0.0508	0.0508	0.00127	0.0762	0.62865	0.03302	0.071997842
0.5588	0.0508	0.00127	0.0762	0.62865	0.03302	2.94251985
0.0508	0.01905	0.009271	0.10795	0.62865	0.03302	3.50E-09
0.5588	0.01905	0.009271	0.10795	0.62865	0.03302	3.52E-09
0.0508	0.0508	0.0127	0.0762	0.62865	0.03302	9.17E-09
0.5588	0.0508	0.0127	0.0762	0.62865	0.03302	2.93402629
0.0508	0.01905	0.00127	0.0127	0.0635	0.05588	8.42E-09
0.5588	0.01905	0.00127	0.0127	0.5715	0.05588	3.23E-09
0.0508	0.0508	0.00127	0.0127	0.0635	0.05588	0.000280012
0.5588	0.0508	0.00127	0.0127	0.5715	0.05588	1.39586659
0.0508	0.01905	0.00127	0.10795	0.0635	0.05588	1.18482784
0.5588	0.01905	0.00127	0.10795	0.5715	0.05588	1.18482784
0.0508	0.0508	0.00127	0.0762	0.0635	0.05588	0.00019255
0.5588	0.0508	0.00127	0.0762	0.5715	0.05588	1.39792937
0.0508	0.01905	0.009271	0.10795	0.62865	0.05588	5.34E-09
0.5588	0.01905	0.009271	0.10795	0.62865	0.05588	2.58010686
0.0508	0.0508	0.0127	0.0762	0.62865	0.05588	2.43E-09
0.5588	0.0508	0.0127	0.0762	0.62865	0.05588	3.11400551
0.1016	0.01905	0.00635	0.0381	0.1524	0.03302	0.000271321
0.5588	0.01905	0.00635	0.0381	0.6096	0.03302	1.67648333
0.1016	0.0508	0.00635	0.0381	0.1524	0.03302	0.000145706
0.5588	0.0508	0.00635	0.0381	0.6096	0.03302	2.24332607
0.1016	0.01905	0.009271	0.0381	0.1524	0.03302	9.88462E-05
0.5588	0.01905	0.009271	0.0381	0.6096	0.03302	1.6583863
0.1016	0.0508	0.0127	0.0381	0.1524	0.03302	4.4751E-05
0.5588	0.0508	0.0127	0.0381	0.6096	0.03302	2.23088836
0.1016	0.01905	0.00635	0.10795	0.1524	0.03302	0.000791172
0.5588	0.01905	0.00635	0.10795	0.6096	0.03302	1.83141127
0.1016	0.0508	0.00635	0.0762	0.1524	0.03302	3.88793E-05

0.5588	0.0508	0.00635	0.0762	0.6096	0.03302	2.3228411
0.1016	0.01905	0.009271	0.10795	0.1524	0.03302	0.000761244
0.5588	0.01905	0.009271	0.10795	0.6096	0.03302	1.06532E-09
0.1016	0.01905	0.00635	0.0381	0.62865	0.03302	2.59429E-08
0.5588	0.01905	0.00635	0.0381	0.62865	0.03302	2.84248461
0.1016	0.0508	0.00635	0.0381	0.62865	0.03302	4.76756E-10
0.5588	0.0508	0.00635	0.0381	0.62865	0.03302	2.84047096
0.1016	0.01905	0.009271	0.10795	0.62865	0.03302	0.062100202
0.5588	0.01905	0.009271	0.10795	0.62865	0.03302	4.36143E-09
0.1016	0.0508	0.0127	0.0762	0.62865	0.03302	1.2532E-08
0.5588	0.0508	0.0127	0.0762	0.62865	0.03302	2.93403306
0.1016	0.01905	0.00635	0.0381	0.1524	0.05588	0.000191114
0.5588	0.01905	0.00635	0.0381	0.6096	0.05588	1.60194208
0.1016	0.0508	0.00635	0.0381	0.1524	0.05588	4.06823E-09
0.5588	0.0508	0.00635	0.0381	0.6096	0.05588	2.29901761
0.1016	0.01905	0.009271	0.0381	0.1524	0.05588	0.000154171
0.1016	0.0508	0.0127	0.0381	0.1524	0.05588	2.27954645
0.5588	0.0508	0.0127	0.0381	0.6096	0.05588	2.27954645
0.1016	0.01905	0.00635	0.10795	0.1524	0.05588	8.28228E-09
0.5588	0.01905	0.00635	0.10795	0.6096	0.05588	6.71419E-09
0.1016	0.0508	0.00635	0.0762	0.1524	0.05588	3.78116E-09
0.5588	0.0508	0.00635	0.0762	0.6096	0.05588	2.41952035
0.1016	0.01905	0.009271	0.0381	0.62865	0.05588	0.004531137
0.1016	0.0508	0.0127	0.0381	0.62865	0.05588	2.74696422
0.5588	0.0508	0.0127	0.0381	0.62865	0.05588	2.74696422
0.1016	0.01905	0.00635	0.10795	0.62865	0.05588	0.09225654
0.5588	0.01905	0.00635	0.10795	0.62865	0.05588	1.86815E-09
0.1016	0.0508	0.00635	0.0762	0.62865	0.05588	0.16990531
0.5588	0.0508	0.00635	0.0762	0.62865	0.05588	3.13327363
0.1016	0.01905	0.00635	0.0381	0.1524	0.03302	0.000102807
0.1016	0.0508	0.00635	0.0381	0.1524	0.03302	0.889243146
0.508	0.0508	0.00635	0.0381	0.5588	0.03302	0.889243146
0.1016	0.01905	0.009271	0.0381	0.1524	0.03302	9.99977E-05
0.508	0.01905	0.009271	0.0381	0.5588	0.03302	0.713801491
0.1016	0.0508	0.0127	0.0381	0.1524	0.03302	4.4751E-05
0.508	0.0508	0.0127	0.0381	0.5588	0.03302	0.937283894
0.1016	0.01905	0.00635	0.10795	0.1524	0.03302	0.000799762
0.508	0.01905	0.00635	0.10795	0.5588	0.03302	0.767483308
0.1016	0.0508	0.00635	0.0762	0.1524	0.03302	4.35142E-05
0.508	0.0508	0.00635	0.0762	0.5588	0.03302	0.972987881
0.1016	0.01905	0.009271	0.10795	0.1524	0.03302	0.000615205
0.508	0.01905	0.009271	0.10795	0.5588	0.03302	6.34201E-09
0.1016	0.01905	0.00635	0.0381	0.5842	0.03302	1.86108E-08
0.508	0.01905	0.00635	0.0381	0.5842	0.03302	1.2956202

0.1016	0.0508	0.00635	0.0381	0.5842	0.03302	4.22098E-09
0.508	0.0508	0.00635	0.0381	0.5842	0.03302	1.29442486
0.1016	0.01905	0.009271	0.10795	0.5842	0.03302	0.037862118
0.508	0.01905	0.009271	0.10795	0.5842	0.03302	4.21894E-09
0.1016	0.0508	0.0127	0.0762	0.5842	0.03302	0.088125826
0.508	0.0508	0.0127	0.0762	0.5842	0.03302	1.35003186
0.1016	0.01905	0.00635	0.0381	0.1524	0.0508	0.000114461
0.1016	0.0508	0.00635	0.0381	0.1524	0.0508	0.946911526
0.508	0.0508	0.00635	0.0381	0.5588	0.0508	0.946911526
0.1016	0.01905	0.009271	0.0381	0.5842	0.0508	0.022692747
0.1016	0.0508	0.0127	0.0381	0.5842	0.0508	1.33094926
0.508	0.0508	0.0127	0.0381	0.5842	0.0508	1.33094839
0.1016	0.01905	0.00635	0.10795	0.5842	0.0508	0.054742744
0.508	0.01905	0.00635	0.10795	0.5842	0.0508	2.30273E-09
0.1016	0.0508	0.00635	0.0762	0.5842	0.0508	0.108144209
0.508	0.0508	0.00635	0.0762	0.5842	0.0508	1.40805575
0.1016	0.01905	0.009271	0.10795	0.5842	0.0508	0.053638266
0.508	0.01905	0.009271	0.10795	0.5842	0.0508	9.99192E-09
0.1016	0.0508	0.0127	0.0762	0.5842	0.0508	0.105536235
0.508	0.0508	0.0127	0.0762	0.5842	0.0508	1.40180213
0.53889	0.05029	0.00662	0.05895	0.61159	0.05588	2.21160274

Appendix C – First Prototype Pickup Prototype Testing Data

The blower and brush settings are controlled on a dial that has numbers from 0-9 followed by the letters A-F. The area in which the debris was distributed is expressed as number of area units occupied by the robot on the floor. The cell marked in grey is the one containing the outlier that was later removed upon further data processing.

Experiment	Filter State	Battle Ship Type	Brush Setting	Blower Setting	Particle Type	Mass Set Down (g)	Area Distributed In	# of Passes	% Picked Up
1	Dirty	2 acrylic rectangles - counterbored	C	F	Flour	50	3	1	64%
2	Dirty	2 acrylic rectangles - counterbored	C	F	Flour	50	2	2	86%
3	Dirty	2 acrylic rectangles - counterbored	C	F	Flour	52	2.5	1	50%
4	Dirty	2 acrylic rectangles - counterbored	C	F	Flour	50	2	1	96%
5	Dirty	2 acrylic rectangles - counterbored	C	F	Flour	50	2	1	66%
6	Dirty	2 acrylic rectangles - counterbored	C	F	Flour	50	2	1	72%
7	Dirty	2 acrylic rectangles - counterbored	C	F	Flour	50	2	1	64%
8	Dirty	2 acrylic rectangles - counterbored	C	F	Flour	50	2	1	64%
9	Dirty	2 acrylic rectangles - counterbored	C	F	Flour	50	2	1	64%
10	Dirty	2 acrylic rectangles - counterbored	C	F	Flour	50	2	1	60%
11	Dirty	2 acrylic rectangles - counterbored	C	F	Flour	50	2	1	54%
12	Dirty	2 acrylic rectangles - counterbored	C	F	Flour	50	2	2	88%
13	Dirty	2 acrylic rectangles - counterbored	C	F	Flour	50	2	2	78%
14	Dirty	2 acrylic rectangles	7	F	Flour	50	2	1	28%

		- counterbored							
15	Dirty	2 acrylic rectangles - counterbored	F	0	Flour	50	2	1	32%
16	Dirty	2 acrylic rectangles - counterbored	F	F	Flour	50	2	1	86%
17	Dirty	2 acrylic rectangles - counterbored	C	F	washer a4 2.5mm	20 (count)	2	1	10%
18	Dirty	1 acrylic rectangle - counterbored	C	F	washer a4 2.5mm & screw	10 each (count)	2	2	10% & 20%

Appendix D - Velocity Measurements

The blower and brush settings are controlled on a dial that has numbers from 0-9 followed by the letters A-F. The location is relative to the images in Figure 21, also reproduced below, such that the right is the right side of the figure and left side is the left of the figure. The greyed out cells contain information that was not used or accounted for in this study but could be useful for further insights or further studies.

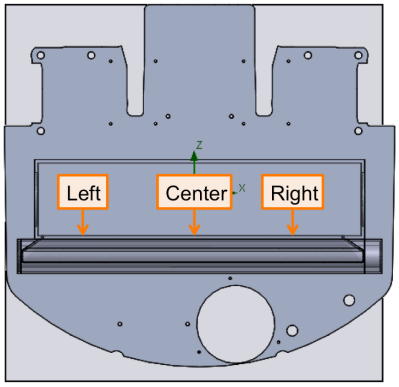

Filter State	Blower Setting	Brush Setting	Location	Air Velocity (m/s)
Dirty	**F**	**C**	**Center of Duct-to-Bin**	**1.8**
Dirty	**F**	**0**	**Center of Duct-to-Bin**	**1.9**
Dirty	D	C	Center of Duct-to-Bin	1.5
Dirty	B	C	Center of Duct-to-Bin	1.3
Dirty	A	C	Center of Duct-to-Bin	1.1
Dirty	9	C	Center of Duct-to-Bin	0.9
Dirty	8	C	Center of Duct-to-Bin	0.8
Dirty	7	C	Center of Duct-to-Bin	0.7
Dirty	6	C	Center of Duct-to-Bin	0.6
Dirty	5	C	Center of Duct-to-Bin	0.5
Dirty	4	C	Center of Duct-to-Bin	0.2
Dirty	E	0	Center of Duct-to-Bin	1.9
Dirty	**F**	**C**	**Right Side**	**2.4**
Dirty	D	C	Right Side	2.2
Dirty	8	C	Right Side	1.7
Dirty	6	C	Right Side	1.2
Dirty	6	0	Right Side	0.6
Dirty	**F**	**0**	**Right Side**	**2.3**
Dirty	**F**	**C**	**Left Side**	**2.1**
Clean	**F**	**C**	**Left Side**	**6.5**
Clean	**F**	**0**	**Left Side**	**6.5**
Clean	D	C	Left Side	5.7
Clean	**F**	**C**	**Center of Duct-to-Bin**	**5.5**
Clean	**F**	**C**	**Center of Duct-to-Bin**	**5.4**
Clean	**F**	**0**	**Center of Duct-to-Bin**	**5.3**
Clean	**F**	**0**	**Right Side**	**6.8**

Clean	**F**	**C**	**Right Side**	**7.2**
Clean	**0**	**C**	**Right Side**	**0**
Clean	**F**	**0**	**Right Side**	**6.3**
Clean	**F**	**C**	**Right Side**	**7.2**
Clean	**F**	**0**	**Right Side**	**7.3**